UCRL-16864

University of California

Ernest O. Lawrence Radiation Laboratory

DETERMINATION OF THE NEUTRON-NEUTRON SCATTERING LENGTH

TWO-WEEK LOAN COPY

This is a Library Circulating Copy which may be borrowed for two weeks. For a personal retention copy, call Tech. Info. Division, Ext. 5545

DISCLAIMER

This document was prepared as an account of work sponsored by the United States Government. While this document is believed to contain correct information, neither the United States Government nor any agency thereof, nor the Regents of the University of California, nor any of their employees, makes any warranty, express or implied, or assumes any legal responsibility for the accuracy, completeness, or usefulness of any information, apparatus, product, or process disclosed, or represents that its use would not infringe privately owned rights. Reference herein to any specific commercial product, process, or service by its trade name, trademark, manufacturer, or otherwise, does not necessarily constitute or imply its endorsement, recommendation, or favoring by the United States Government or any agency thereof, or the Regents of the University of California. The views and opinions of authors expressed herein do not necessarily state or reflect those of the United States Government or any agency thereof or the Regents of the University of California.

UCRL-16864

UNIVERSITY OF CALIFORNIA

Lawrence Radiation Laboratory
Berkeley, California

AEC Contract No. W-7405-eng-48

DETERMINATION OF THE NEUTRON-NEUTRON SCATTERING LENGTH

Edward Shield
(Ph. D. Thesis)

December 19, 1966

B. Results and Errors

1. χ^2 Distributions and Errors 36

2. Standard Deviation and Probable Error of a_{nn} . . 42

C. Experimental Errors

1. Detector Angle and Target Pressure 43

2. Beam Energy Determination 45

3. Channel Energy Width 46

4. Angular Dependence - $|g(\theta)|^2$ 47

5. Energy Resolution 47

V. Discussion

A. Long Range and Short Range Production 49

B. Correlation Experiments. 56

C. The Reaction $He^3(d,t)2p$ 59

D. Determination of the n-n Scattering Length from the Reaction $\pi^- + D \rightarrow n + n + \gamma$ 60

Acknowledgements 61

Appendices

A. Phase Space Energy Dependence 62

B. Calculation of Jacobian Transformation 63

Footnotes and References 65

DETERMINATION OF THE NEUTRON-NEUTRON SCATTERING LENGTH*

Edward Shield

Lawrence Radiation Laboratory
University of California
Berkeley, California

ABSTRACT

Measurements on the reaction $T(d,He^3)2n$ at 32.7 MeV incident deuteron energy have been used to determine the n-n scattering length. Watson's theory of final state interactions provides a theory with which the experimental data giving the number of He^3 at 6 and 8 deg versus energy can be compared. Comparison is made with numbers of He^3 near the maximum energy in which case the neutrons go off with little relative energy under the influence of a final state s-wave interaction. The best fit of the data to theory gives $a_{nn} = -16.1 \pm 0.1$ F. The applicability of this method is proved by measurements on the reaction $He^3(d,T)2p$ which gives a value for a_{pp} equal to the accepted value within the experimental errors. Comparisons of results with other measurements of a_{nn} are given.

action calculational methods now available. These are potential models calculated from field theoretical treatments of particle exchanges, e.g., π, ρ, etc. and the construction of scattering amplitudes using dispersion theory.

The application of final state interaction theory for the accurate determination of scattering parameters is in practice a not unequivocal procedure. One specific difficulty is that the primary interaction (or production process) which in the theory is independent of the relative energy of the interacting pair at small relative energy, may not in fact be so. For example, this seems to be the case for the reaction $p + d \rightarrow n + n + p$ at n-n relative energies of 1 MeV and greater. This severe limitation is due to the long-range nature of the primary interaction, and will be discussed below.

Another problem encountered is that of multiple final state interactions in the presence of three strongly interacting particles. These are quite evident in the spectra of the p + d reaction at low bombarding energies.[14] Since the cross-section enhancements are strongest at the lowest relative energies of each pair, kinematically, for sufficiently large total center of mass energies the different pair interactions should be completely separable (excluding the possibility of resonant states). Nevertheless this is a complication that must be noted.

In this work, a determination of the neutron-neutron scattering length through the final state enhancement of the He^3 spectrum of the reaction $H^3(d,He^3)2n$ at 32.7 MeV and $\emptyset_{lab} = 6$ deg is presented and discussed. The theoretical background, experimental procedure and method of analysis are described. The discussion attempts to deal with some of the points raised in the preceding paragraphs.

II. THEORETICAL BACKGROUND

A. Final State Interactions-Factored Wave-Function Enhancement

In the original paper on the subject of final state interactions,[1] Watson considered processes which could be described by a Hamiltonian with two separable potentials, $H = H_0 + U + V$. Here V is considered a production potential, an interaction connecting two channels, a and b. In the important special case where U acts only between particles of the outgoing channel and does not connect a and b, he showed that the transition matrix for the process could be written

$$T_{ab} = \langle \phi_b^{(-)} | V | \psi_a^{o(+)} \rangle \tag{1}$$

where

$$\psi_a^{o(+)} = \chi_a + [E_a - H_o + i\epsilon]^{-1} V\psi_a^{o(+)}$$

and

$$\phi_b^{(-)} = \chi_b + [E_b - H_o - i\epsilon]^{-1} U\phi_b^{(-)}$$

with χ the plane-wave eigenfunctions of H_o. If U acts only between a pair of particles in the final state, say "1" and "2," then

$$\phi_b^{(-)} = h_{B'}^{(-)}(\epsilon')g_q^{(-)}(r) \tag{2}$$

where B' and ϵ' do not contain q or r and $g_q^{(-)}(r)$ describes the relative motion of "1" and "2." (1) becomes

$$T_{ba} = \int d^3r g_q^{(-)}(r) \int d^3\epsilon' h_{B'}^{(-)}(\epsilon')V\psi_a^{o(+)} . \tag{3}$$

It is assumed that q, the relative momentum of "1" and "2" is sufficiently small so that g is s-wave. Therefore, asymptotically

$$g_q^{(-)} = e^{-i\delta}[\sin(qr + \delta)]/qr.$$

The domain of integration of (3) is determined by the non-zero values of $V\psi_a^{o(+)}$; if this range is sufficiently small, then $qr \ll 1$. (This condition of short-range production[11] will be discussed in Sec. V. A.) So,

$$\sin(qr + \delta) \simeq \sin\delta(qr \cot\delta + 1)$$

$$= \sin\delta \left[1 - \frac{r}{a} + \frac{1}{2}r_o q^2 r\right] \tag{3a}$$

where a is the scattering length and r_o the effective range. Ignoring the q^2 term, $g_q^{(-)}$ may be written

$$g_q^{(-)}(r) \simeq e^{-i\delta}\,[(\sin\delta)/q]f(r). \tag{4}$$

Inside the range of U, which is assumed strong and attractive, $g_q^{(-)}(r)$ does not depend strongly on q for small q, except through the boundary condition where it joins the outside wave function. Therefore, (4) is valid inside the region of interaction as well as outside of it, for small q. Therefore, (3) now becomes

$$T_{ba} = \frac{e^{-i\delta}\sin\delta}{q}\int d^3r d^3\epsilon\; f(r)V\psi_a^{o(+)} \tag{5}$$

and the cross section for an n particle state is[15]

$$d\sigma = \frac{2\pi}{\hbar v_{rel}}\int \delta\left(\sum_{i=1}^{n} W_i - E_a\right)\delta\left(\sum_{i=1}^{n} p_i\right) \times \prod_{i=1}^{n}\left(d^3p_i/h^3\right)\sum_{spins}|T_{ba}|^2 . \tag{6}$$

For the three particle final state, after integration over the momentum and energy delta functions we have

$$\frac{d^2\sigma}{d\Omega dE} = \frac{8\pi^2}{\hbar v_{rel}}\,\rho(E)\sum_{spins}|T_{ba}|^2 , \tag{7}$$

where $\rho(E)$, the phase space factor, may be defined from

$$\rho(E_1)dE_1 d\Omega_1 d\Omega_{23} dE_2 = \left[d^3p_1 d^3p_2\right]/h^6 .$$

The phase-space factor corresponding to (7), the differential cross section for observation of a single particle is

$$\Omega(E_1) = 2/h^6 \left[\frac{m_1{}^3 m_2 m_3}{M}\right]^{1/2} \left[E_1\right]^{1/2} \left[E_1{}^{max} - E_1\right]^{1/2} .$$

We may rewrite (5) in the form

$$|T_{ba}|^2 = \frac{1}{\left(q^2 + q^2 \cot^2\delta\right)} |T_{ba}{}^{(o)}|^2 , \tag{8}$$

where $T_{ba}{}^{(o)}$ is the integral in (5) and is independent of q. In the specific case of the reaction, $H^3 + d \rightarrow 2n + He^3$, we have in the c.m. system

$$d^2\sigma/d\Omega dE = \frac{|g(\theta)|^2 \left[(E)(E^{max} - E)\right]^{1/2}}{E_{nn} + \hbar^2/m_n \left[-1/a + r_o q^2/2\right]^2} , \tag{8a}$$

where we have absorbed all constants and $|T_{ba}{}^{(o)}|^2$, which is assumed to depend only on θ, into the factor $|g(\theta)|^2$. The Jacobian of the transform of (8a) to the laboratory is simply $\left(E_{lab}/E\right)^{1/2}$. (This as well as the phase-space expression is derived in the Appendix.)

It remains to show that $T_{ba}{}^{(o)}$ is essentially the same transition matrix element that one would obtain if there were no strong final state interaction present. Also it will be noticed that the "enhancement," $\sin^2\delta/q^2$, approaches zero for large relative energies of the interacting particles, and consequently so does $d^2\sigma/d\Omega dE$. This is certainly unrealistic; what should occur is that when the enhancement becomes small, the cross section approaches the unenhanced cross section. In other words, the

enhancement factor should become unity as the final state interaction becomes weak. Such an enhancement factor can be defined by the use of Jost functions.

B. Jost Function Enhancement

The Schrödinger equation for s-wave scattering is

$$\left[- \frac{d^2}{dr^2} + V(r) - k^2 \right] w_o(k,r) = 0, \tag{9}$$

where w_o is a solution simply related to ψ_o, the solution with physical boundary conditions by

$$\psi_o = e^{-i\delta_o} \frac{w_o(k,r)}{kr} .$$

It is convenient to introduce a function which is a solution to (9), but which satisfies the same boundary conditions as the solutions to the "free" Schrödinger equation with V = 0. These are

$$\phi(k,0) = 0, \tag{10a}$$

$$\phi'(k,0) = 1. \tag{10b}$$

ϕ is related to ψ_o by

$$\phi(k,r) = \frac{1}{\alpha} \psi_o(k,r).$$

$\phi(k,r)$ is a real function for real k, and is even in k. Also it is everywhere analytic in the k-plane.

The Jost function, f(k,r), is defined as a solution to (9) with the boundary condition

$$\mathrm{Lim}_{r \to \infty} e^{ikr} f(k,r) = 1. \tag{11}$$

From Eq. (11) we have for real k,

$$f^*(-k,r) = f(k,r). \tag{12}$$

We may construct solutions regular at the origin from the two linearly independent solutions $f(k,r)$ and $f(-k,r)$.

$$\phi(k,r) = \frac{1}{2ik}\left[f(k)f(-k,r) - f(-k)f(k,r)\right], \tag{13}$$

where

$$f(\pm k) = f(\pm k,0).$$

From Eqs. (11) and (13)

$$\phi \xrightarrow[r \to \infty]{} \frac{1}{2ik}\left[f(k)e^{ikr} - f(-k)e^{-ikr}\right] \tag{14}$$

$$= \frac{f(-k)}{2ik}\left[-e^{-ikr} + \frac{f(k)}{f(-k)}\, e^{ikr}\right],$$

$$\psi_{k,o}(r) \to \frac{\sqrt{2/\pi}}{2ikr}\left[-e^{-ikr} + S_o(k)e^{ikr}\right]. \tag{15}$$

Comparing (14) and (15),

$$S_o(k) = \frac{f(k)}{f(-k)} \tag{16}$$

but

$$S_o(k) = e^{2i\delta_o(k)}.$$

Therefore, from (12) and (16)

$$f(k) = |f(k)|e^{i\delta_o(k)}.$$

Also comparing (14) and (15)

$$\alpha = \left[(\pi/2)^{1/2}\ \frac{|f(-k)|}{k}\right]^{-1}.$$

By using the boundary condition (10b), the ratio

$$F' \equiv \left.\frac{w_o(k,r)}{\sqrt{\frac{\pi}{2}}\ \sin kr}\right|_{r=0}$$

is found to be

$$F' = \frac{1}{|f(k)|} \ .$$

Using the quantity F', the ratio, at r = 0, of the value of the s-wave function in a potential to the value of the wave function for no interaction, may be found. Thus

$$F \equiv \frac{\psi_{k,o}(k,r)}{\psi_{k,o}^{(o)}(k,r)} = \frac{e^{i\delta_o(k)}}{|f(k)|} \ . \tag{17}$$

$|F|^2$ therefore represents the ratio of the probabilities of finding the two particles at r = 0 with and without an interaction between them. It is, for this reason, called an enhancement factor. The important distinction between the Jost function enhancement factor, and the factor* $(\sin\delta)/k$ of (8a) is that the former has a more appropriate normalization. It can be shown that $|F|^2 \to 1$ as $k \to \infty$;[16] this means that as the final state effects become small, the cross section approaches the (unenhanced) production cross section, and not zero, as $(\sin\delta)/k$ does.

From an integral representation of f(k) in terms of the scattering phase shift,[16] it can be shown that, in the effective range approximation

$$f(k) = \frac{k - i\beta}{k - i\alpha} \ , \tag{18}$$

where

$$\frac{1}{2} r_e(\alpha-\beta) = 1$$

$$\frac{1}{2} r_e \alpha \beta = - 1/a \ .$$

Therefore,

$$|F|^2 = \frac{k^2 + \alpha^2}{k^2 + \beta^2} \ . \tag{19}$$

* k and q are used interchangeably.

It is interesting to compare this enhancement factor with that obtained from the factored wave-function approach.

$$\frac{\sin^2 \delta}{k^2} = \frac{k^2 + \alpha^2}{k^2 + \beta^2} \frac{1}{\left(k^2 + \alpha^2\right)} \quad . \tag{20}$$

In the region $k^2 \ll \alpha^2$, the energy dependence of (19) and (2) become equivalent. However, for the neutron-neutron system, $\alpha^2 = 66.0 \times 10^{24} \text{cm}^{-2}$, while a relative energy of 1 MeV corresponds to $k^2 = 2.41 \times 10^{24}$ cm^{-2}; thus for the purpose of accurate determination of scattering parameters the two approaches are not equivalent.

C. Coulomb Effects

The asymptotic solution to the Schrödinger equation with a Coulomb potential is

$$\phi_f^{(-)} = e^{-i\delta}\left[F_o \cos \delta + G_o \sin \delta\right]/kr \quad .$$

For $kr \ll 1$

$$\phi_f^{(-)} \approx e^{-i\delta} \sin \delta \left[1 - r/a\right]/Ckr, \tag{21}$$

where we have used the effective range expansion with Coulomb terms, and ignored terms of order k^2r^2,

$$C^2 k \cot \delta = -1/a - \frac{h(\eta)}{R} + \frac{ro}{2} k^2 \ , \tag{22}$$

$$C^2 = \frac{2\pi\eta}{e^{2\pi\eta}-1} \quad ; \qquad \eta = \frac{1}{2kR} \quad ; \qquad R = \frac{\hbar^2}{m_p e^2}$$

$$h(\eta) = \text{Re}\left[\frac{\Gamma'(1 - i\eta)}{\Gamma(1 - i\eta)}\right] - \ln\eta \ .$$

Therefore,

$$\phi_f^{(-)} \simeq \frac{e^{-i\delta} \sin \delta}{Ck} f(r) . \tag{22a}$$

Which is of the same form as Eq. (4). Therefore, in the case of the final state interaction between two protons, the cross section is

$$\frac{d^2\sigma}{d\Omega dE} = \left|g(\theta)\right|^2 \frac{C^2[E(E^{max} - E)]^{1/2}}{C^4 E_{2p} + \frac{\hbar^2}{m_p}\left[-\frac{1}{a_p} - \frac{h(\eta)}{R} + \gamma E_{2p}\right]^2} , \tag{23}$$

where

$$\gamma = \frac{r_o m_p}{2\hbar^2} .$$

III. EXPERIMENTAL

A. Beam Optics and Alignment

For this experiment deuteron beams of 32.7 and 40.4 MeV were obtained from the Berkeley 88-inch sector-focused cyclotron. The beam line and orientation of magnets is shown in Fig. 1. In the horizontal plane the quadrupole Q_1 focuses the beam between itself and the switching magnet, which then bends the beam through 40 deg. Q_2 was then used to obtain a focal point at the analyzing slit. This slit was 0.070-in. wide. The rays from the image source were then focused at the target center by Q_3. In the vertical plane the beam remains parallel between the switching magnet and Q_3, which focuses it at the target center. Initially, the beam spot was observed visually on a quartz plate at the target center position. Before obtaining the beam, the 0.070-in. wide entrance collimator, the target center, and the counter collimator in its 0 deg position had been optically aligned. To obtain a beam line coincident with the line defined by these points, horizontal beam profiles were made (see Fig. 2) by sweeping a 0.100-in. wide slitted tantalum plate on one counter arm through the beam. By moving slowly through a small range of angles near 0 deg, the beam profile is obtained as the beam current which reaches the Faraday cup directly behind the slit as a function of angle. The whole scattering chamber could then be rotated about the entrance collimator to center the beam.

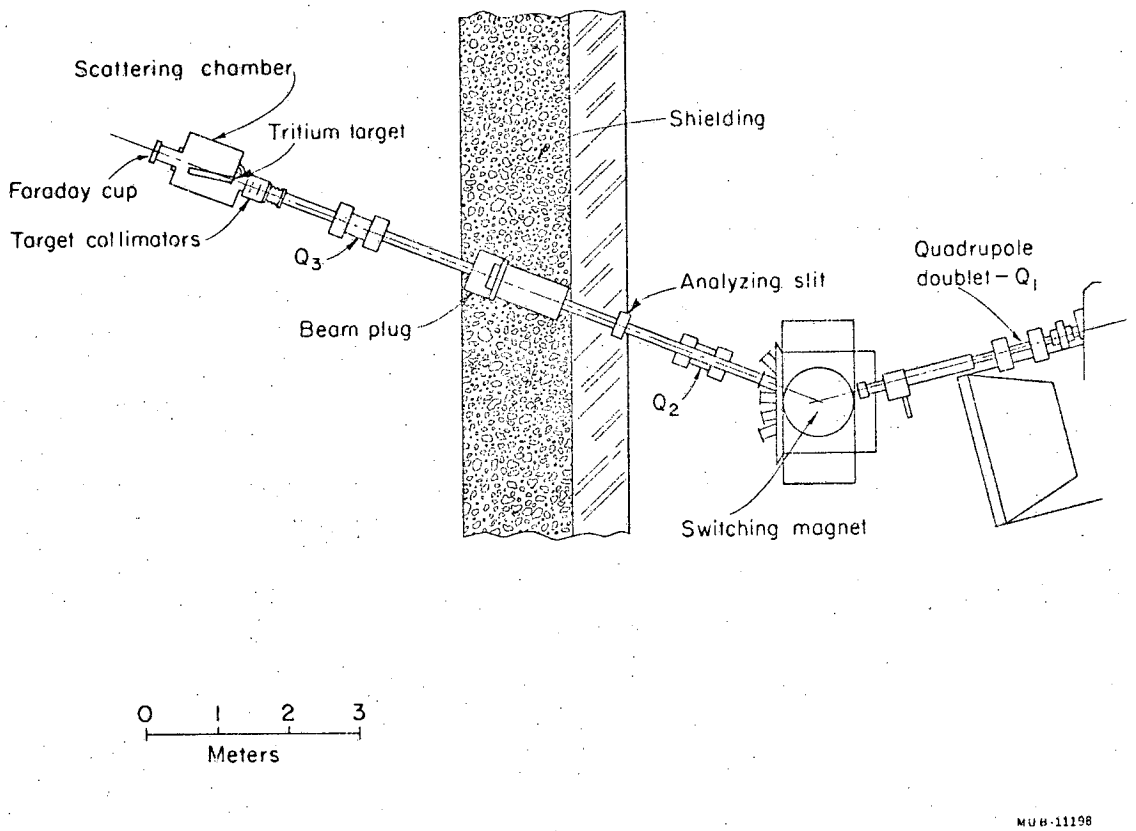

Figure 1. Experimental layout.

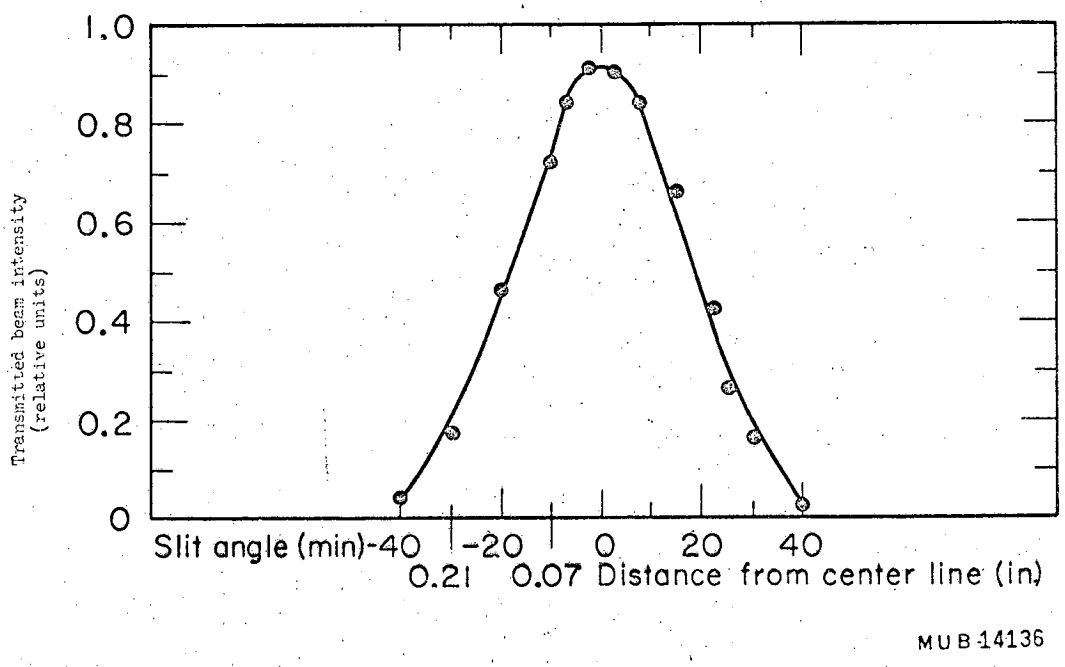

Figure 2. Horizontal beam profile.

B. Gas Target and Tritium Filling System

The gas target is shown in Fig. 3. It was constructed in two tandem horizontal sections, and during the experiment was placed in a 20-in. portable scattering chamber. The scattering chamber and target were evacuated to a pressure of approximately 10^{-5} mm of mercury. The upper section of the target was filled when the target was already in the scattering chamber, through an external fill line. The lower section was filled and isolated previous to placing the target in the chamber; this section contained either He^3 or H^3. Generally the upper section was filled with N^{14} at 1/3 atmosphere or evacuated for background runs.

The target was constructed in an unusual wedge-shape to minimize its volume, so that large amounts of H^3 would not be required. The volume of each of its chambers was 65 cc. The entrance and exit windows were constructed of 0.00041-in. thick "Havar" foil and were soldered to the target body. It was found that this was the minimum thickness that could consistently tolerate a differential pressure of 1 atmosphere.

In order to avoid the necessity of pumping on the tritium gas during the experiment, we filled the H^3 target section outside the scattering chamber, by simply allowing the evacuated target and coupled H^3 gas container to reach equilibrium. In this way we obtained a tritium pressure of 0.2 atmospheres (about 40 curies). This relatively low pressure was more than adequate, since for optimal energy resolution we were limited to low counting rates by the electronics.

C. Counter Collimator System

The detector, counter collimator and target system are shown in Figs. 4a and b. The counter collimator system (see Fig. 5) was

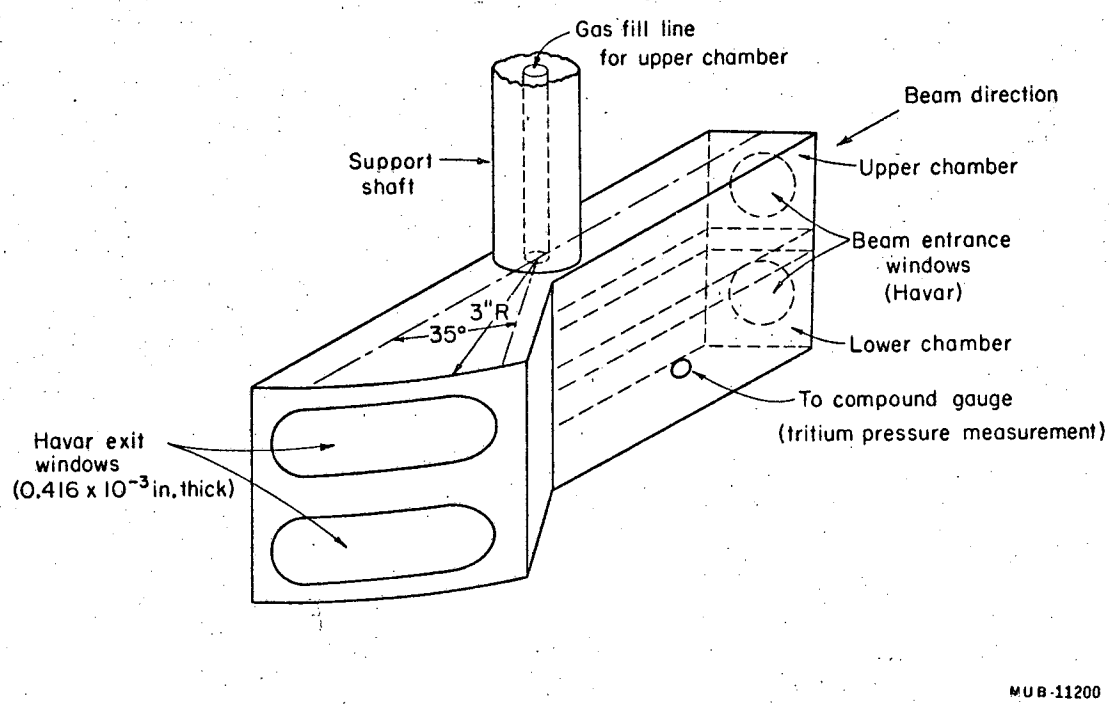

Figure 3. Gas target chamber.

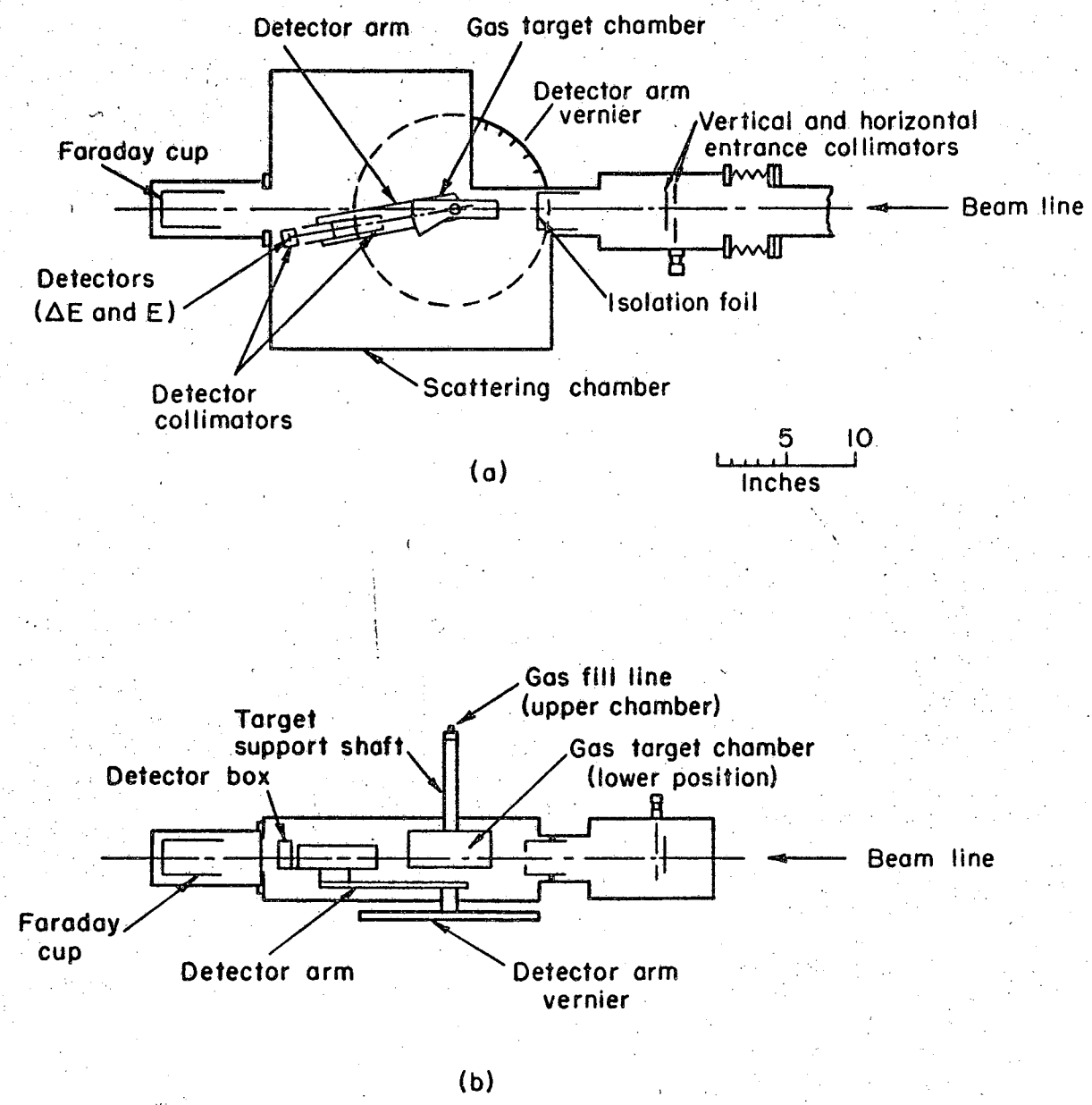

MUB-11199

Figure 4. Detector and target system.

(a) Top view (b) Side view

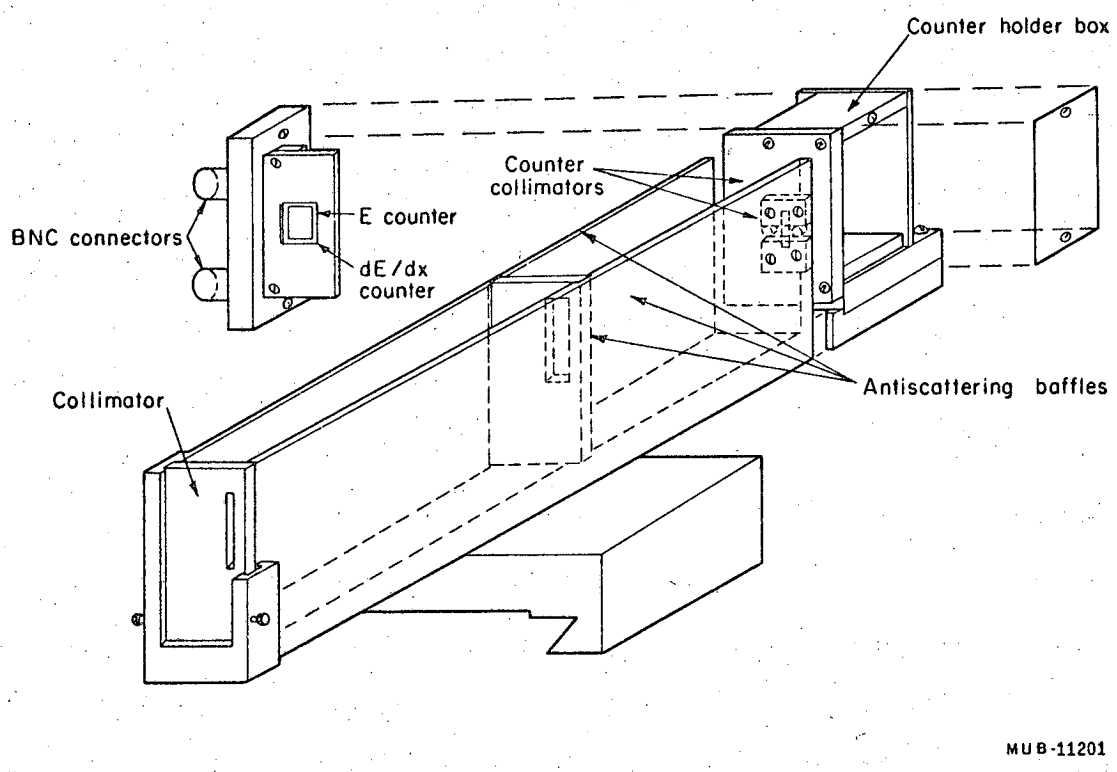

Figure 5. Detector holder and collimating system.

designed to reach small-scattering angles (~ 3 deg). The ultimate limitations in reducing the angle of observation were the spread of the direct beam behind the target, and elastic scattering from the target entrance window. The tantalum counter collimator thicknesses (0.040-in.) were such as to stop 25 MeV protons; their widths (0.070-in.) were determined by the need for relatively good angular resolution (we obtained approximately ± 0.3 deg) without undue sacrifice of counting rate.

D. Beam Energy

The aluminum foils used as absorbers in determining the range of the beam deuterons were discs turned to an accuracy of better than 0.1% of their diameters. Their weight was determined on a microbalance to an accuracy of better than one part in 100,000. The impurity content was less than 0.1% by weight. However, the beam energy was measured in air and there were air gaps both before and after the passage through the foils. The values used are given in Table I, where the energy losses are summarized. The ranges of deuterons in aluminum, nitrogen and oxygen were obtained from the work of Williamson and Boujot.[17] A representative range curve is given in Fig. 6.

Table I. Beam energy measurement.

Material	Thickness (cm.)	Aluminum Equivalent (mg/cm^2)	E (MeV)	Uncertainty (mg/cm^2, Al)
Air	9.66	13.4	32.7	± 0.5
Al		750.2		± 4.2
Air	6.10	8.6	6.0	± 0.9
Al		33.0		
Total		805.2 mg/cm^2 ± 5.6	E = 32.69 MeV ± 0.13	

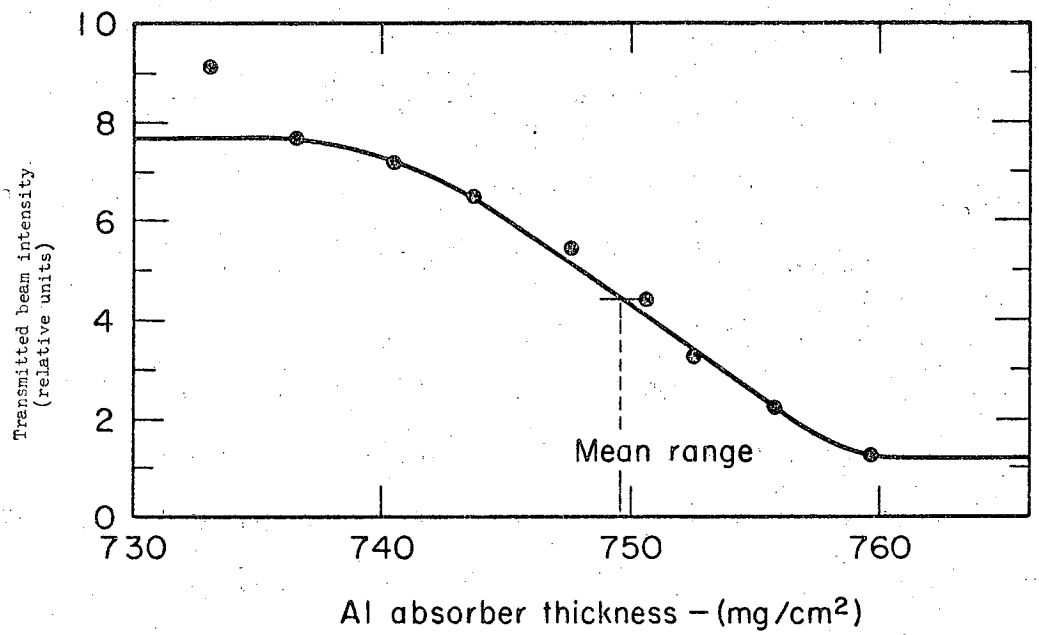

MUB-11202

Figure 6. Range-energy curve.

E. Detectors

The ΔE detector used was a specially prepared phosphorus-diffused-in-silicon type. The depleted (charged-particle sensitive) layer of this detector was 0.0036-in. thick at the reverse bias operating voltage of 80 volts. The non-depleted "dead" layer of this type of detector is less than 1μ thick.[18]

The E detector was a lithium-drifted-silicon type. Its depletion layer was 0.083-in. thick operated at 225 to 250 volts reverse bias.

F. Electronics

A schematic diagram of the electronics is given in Fig. 7.

1. General Description

The detector signals were fed directly through low capacity cables into each of two charge sensitive preamplifiers. The output signal of these preamplifiers is independent of detector capacitance and was of the order of 0.5 volts.

Both pulses, ΔE and E, were next fed into linear pulse amplifiers, whose maximum gains are about 1000X. This amplifier contains shaping networks. An L-R integrator was used to give the output pulse 0.2 μsec rise time. These pulses were then clipped to about 3 μsec by the amplifier's delay line circuit which superposes an inverted delayed pulse of the same amplitude on the original pulse. In addition there was a slow coincidence requirement between ΔE and E pulses for output. The net amplification of the input signals was approximately 10X. The output is then fed to the identifier unit.

2. Identifier

By using the empirical range-energy relation for charged particles,

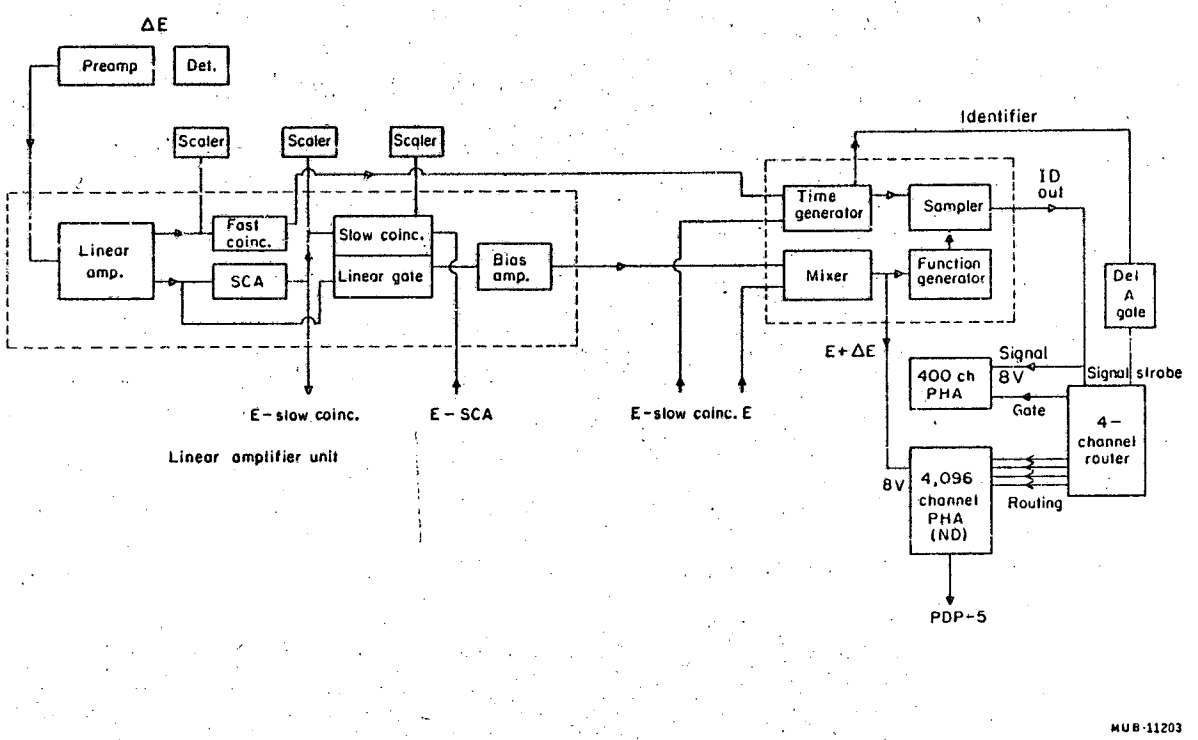

Figure 7. Electronics schematic. Only one of the two linear amplifier systems is shown.

$R = aE^{1.73}$, the identifier generates a pulse whose amplitude is dependent only on the type of particle detected.[19] The operation of this unit is briefly outlined below.

a. Mixer. The E and ΔE signals are fed first into the gated mixer circuit. Essentially this unit adds a shortened ΔE signal, delayed by 1.5 μsec by the timing generator, to the last 1.5 μsec of the E pulse. Thus the output is a stepped wave form of amplitude E and then $E + \Delta E$. The $E + \Delta E$ pulses are analyzed and stored in the Nuclear Data PHA.

b. Function Generator. This unit electronically simulates the range-energy relation and generates a stepped wave form of amplitude $E^{1.73}$ and $(E + \Delta E)^{1.73}$.

c. Sampler. This unit "samples" the step signal of the function generator at 1.5 μsec and 2.5 μsec and forms the difference

$$(E + \Delta E)^{1.73} - E^{1.73} = T/a,$$

where T is the thickness of the ΔE detector. The constant a is inversely proportional to the value MZ^2 of the particle, and the amplified output of the sampler is the "identifier" output signal. Shown in Fig. 8 is a typical identifier spectrum as displayed on the RIDL 400 channel PHA. This spectrum was used for the identification of He^3 from $d + T \rightarrow 2n + He^3$; protons and deuterons from other channels were not in range of the total detector thickness and so their identification was quite poor. Ordinarily, good separation of all particles is readily obtained.[19] Here we have excellent separation between tritons, He^3 and He^4.

3. Routing

The identifier output signals of the sampler were used to route $E + \Delta E$ signals from the mixer to the appropriate one of four quadrants of

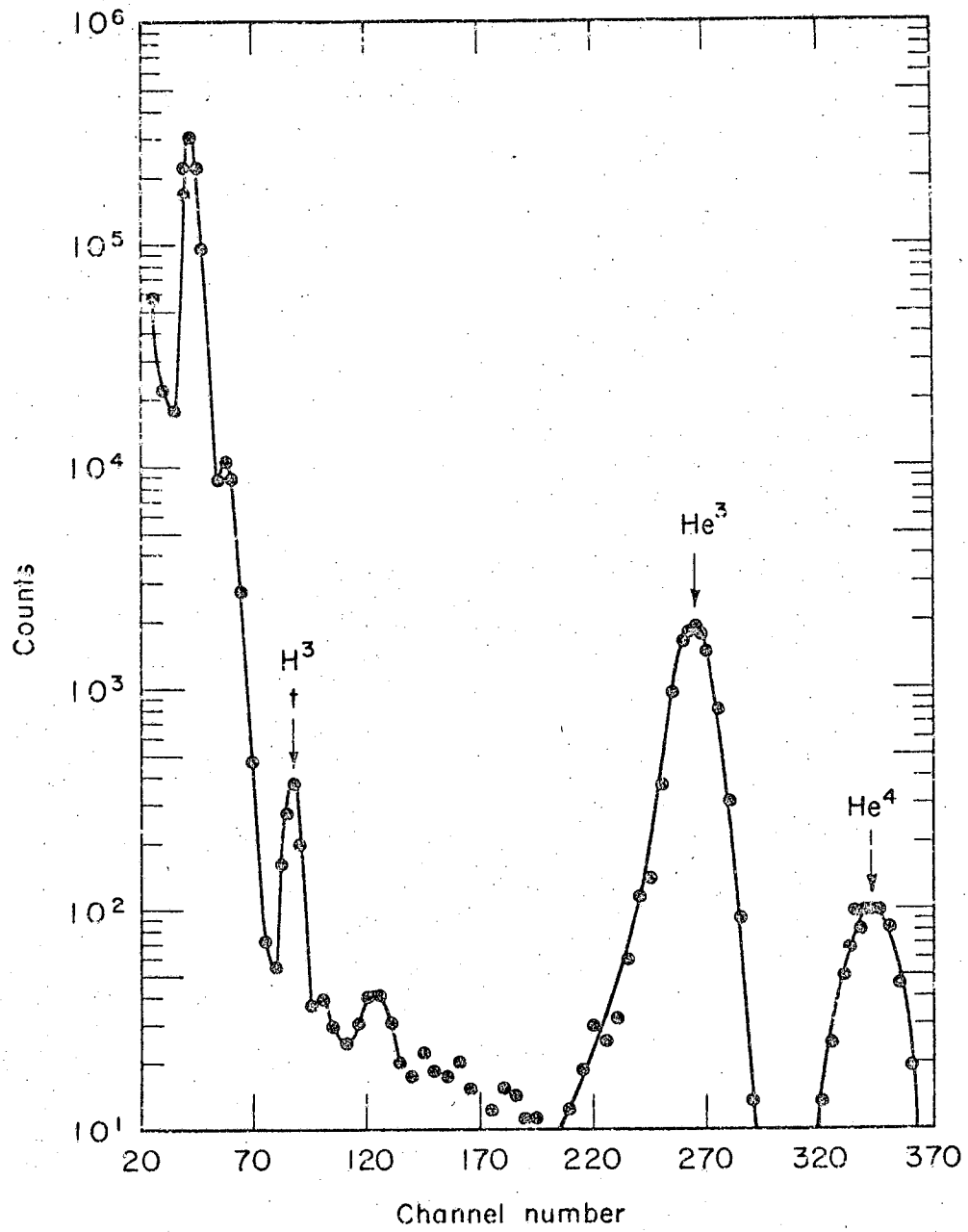

MUB-11204

Figure 8. Particle identifier spectrum.

a 4096 channel Nuclear Data PHA. The range of identifier spectrum amplitudes which would generate a routing signal in one of the four router channels was determined by setting the upper and lower windows of a separate single channel analyzer on the identifier peak of the desired particle as observed on the RIDL display. These routing signals then initiated storage of the $E + \Delta E$ pulse. The $E + \Delta E$ spectra were finally transferred to a PDP-5 on-line computer which stored them on magnetic tape, printed, and plotted them.

IV. ANALYSIS

A. Calculations

1. P. H. A. Channel Energy Width

The first step in the reduction of the data was the determination of a relative energy scale by calibration of the channel energy width of the Nuclear Data pulse-height analyzer. The channel energy width is the difference of two energies corresponding to adjacent storage channels for input pulses. The discrete spectra of the reactions $N^{14}(d,He^3)C^{13}$ and $N^{14}(d,t)N^{13}$ were used for this purpose.[20] Shown in Figs. 9 and 10 are the He^3 spectra from $N^{14}(d,He^3)C^{13}$ at E_d = 32.7 MeV, θ_{lab} = 6 deg and θ_{lab} = 20 deg. A program called "Lycurgus"[21] was used to calculate the kinematics of the ground state and excited states of C^{13}. The channel width was then calculated from the separation between the ground state and each of four well-resolved levels. The average channel width was found to be 34.21 KeV/channel. At E_d = 40.4 MeV this channel width increased due to lower gain settings of the amplifiers and was determined to be 40.9 KeV/channel with a maximum deviation of $\pm$ 0.2 KeV/channel.

2. Target Center Channel Energy Width

Due to the considerable variation of energy loss with energy for He^3 particles in the Havar foil exit window of the gas target, the channel energy width at the target center, where the events take place, is different from the corresponding channel energy width. From the definition above, choosing the observed energies E_1 and E_2, corresponding to the lower edges of the adjacent channels, the observed channel width is

$$\Delta E_{ch} = E_2 - E_1 = E'_2 - E'_1 - (\delta E_2 - \delta E_1) ,$$

where E'_1 and E'_2 are the target center energies and δE_1 and δE_2 are the

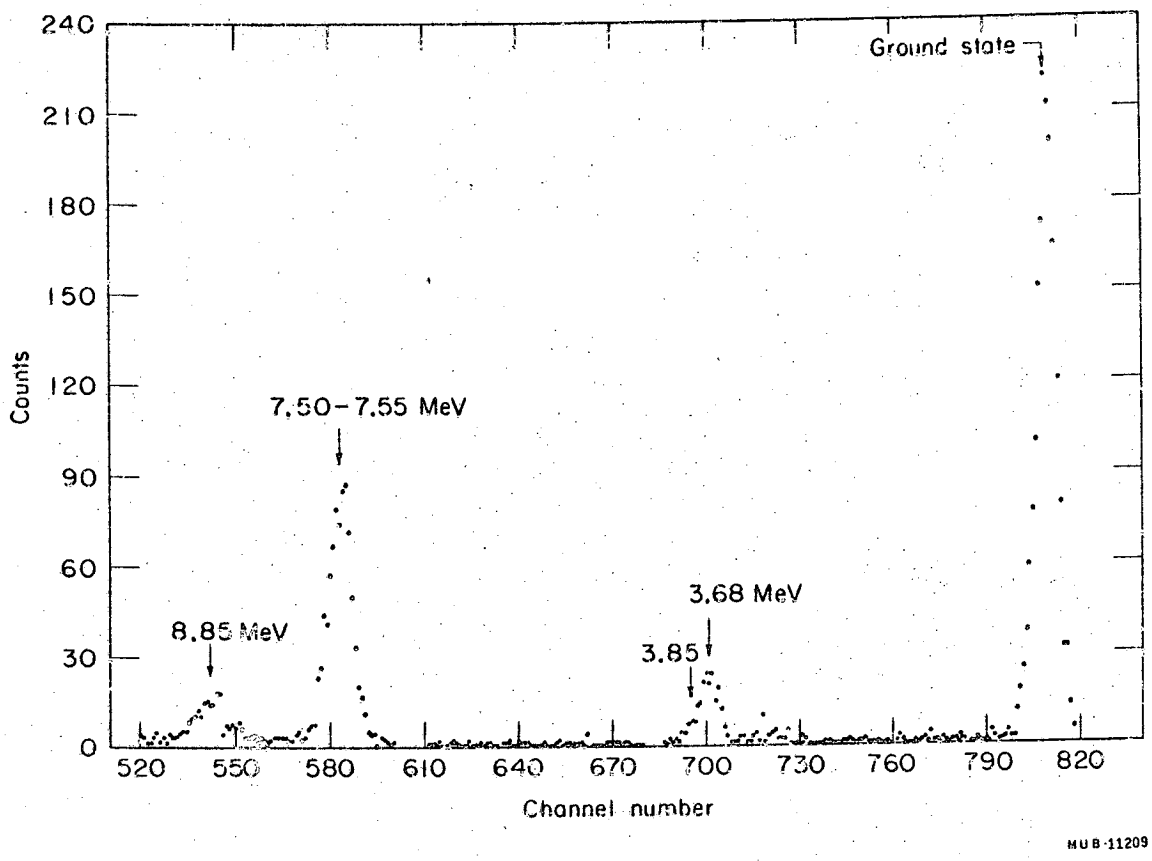

Figure 9. 6 deg spectrum of He^3 from $N^{14}(d,He^3)C^{13}$.

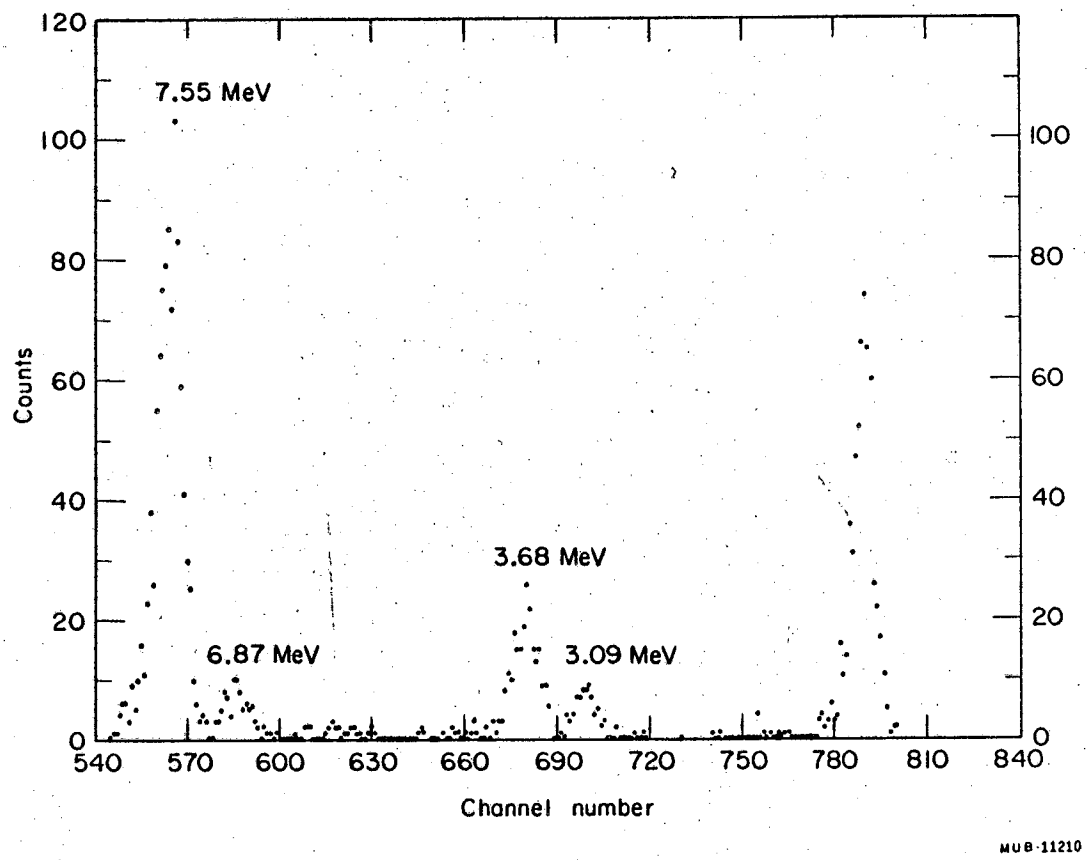

Figure 10. 20 deg spectrum of He^3 from $N^{14}(d,He^3)C^{13}$.

corresponding total energy losses in target gas and Havar foil.

The differential energy loss of the He^3 particles in the gas or foil may be written

$$\delta E = S(E) \cdot \rho x \ ,$$

where $S(E)$ is the stopping power of the material, ρ its density and x its thickness. The difference in energy losses for particles of energy E'_1 and E'_2 is

$$\delta E'_2 - \delta E'_1 = - \left[S_1(E'_2) - S_1(E'_1) \right] (\rho x)_1$$
$$= - \Delta S_1 \cdot (\rho x)_1 \ .$$

The index 1 on the stopping power and thickness denotes the first energy loss (in thetarget gas for this case). For $E'_2 - E'_1 \ll E'_2$,

$$\Delta S_1 = + D_1(E'_1)(E'_2 - E'_1),$$

where $D(E')$ is the derivative of $S(E')$. Thus the channel width after the particles have passed through a thickness, x_1, of material is

$$\Delta E''_{ch} = \Delta E'_{ch} - D_1(E')\Delta E'_{ch} \cdot (\rho x)_1 \ , \tag{24}$$

where $\Delta E'_{ch}$ is the target center channel energy width. By applying this formula to the second energy loss (in the Havar foil) we obtain

$$\Delta E'_{ch} = \left\{ \Delta E_{ch} / \left[1 - D_2(E'') \cdot (\rho x)_2 \right] / \left[1 - D_1(E') \cdot (\rho x)_1 \right] \ , \right. \tag{25}$$

where $(\rho x)_2$ is the thickness of the Havar foil and E'' the particle energy when entering the foil. If only the observed energy is known, as is the case here, there is no simple procedure to find the particle energy prior to the large energy losses. The advantage of (25) is that approximate energies for E' and E'' may be used to determine $\Delta E'_{ch}$; fortunately, in

the energy range we considered, the variation of $\Delta E'_{ch}$ with energy is quite small (about .3% over the full energy range) and for ease of calculation it was considered a constant. For example, at 6 deg, E_d = 32.7 MeV, $(\Delta E)_{ch}$ was found to be 33.25 KeV/channel.

3. Angular Distributions

In order to define angular distributions for a three-particle final state it is necessary to specify the particle energies at which the spectrum is evaluated, as well as the energy intervals integrated over. In (8a) we have assumed a c.m. cross section separable in energy and angular dependence, contained in $|g(\theta)|^2$. To determine $|g(\theta)|^2$ we define

$$\left.\frac{d\sigma}{d\Omega}\right|_{E_{nn}} \equiv \int_{E_1}^{E_2} \frac{d^2\sigma}{d\Omega dE}\, dE \quad . \tag{26}$$

However, only relative values of $d\sigma/d\Omega$ are necessary. Therefore, the quantity calculated was

$$S = N \sin\theta/\mu C \quad , \tag{27}$$

where N is the number of counts in the interval $E_2 - E_1$, θ the lab angle and μC the number of microcoloumbs collected in the Faraday cup. S was evaluated for three fixed values of E_{nn}, at lab angles 6, 8, 10, 15, and 20 deg. The variation of S with $\theta_{c.m.}$ is due only to the $|g(\theta)|^2$ factor in the cross section of (8a), if the energy interval of integration in (26) is sufficiently small and E_{nn} is fixed. In fact, the intervals were five channels (171 KeV) wide (the resolution FWHM was seven channels). These intervals were centered about each of the three values of E_{nn} shown in Fig. 11. Therefore, we assumed

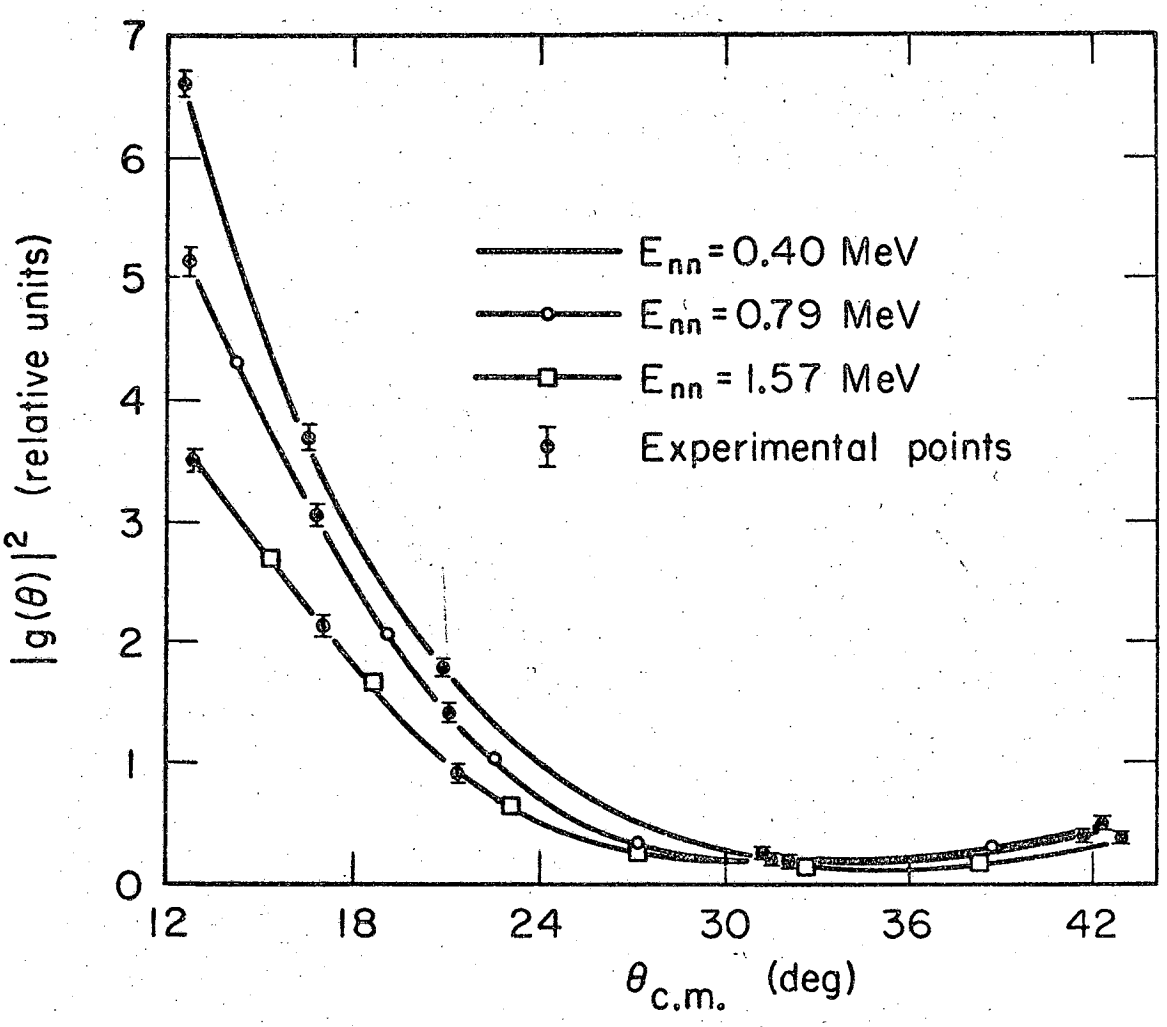

MUB-11205

Figure 11. $|g(\theta)|^2$ calculated from a 0.170 MeV interval centered at three spectral points.

$$|g(\theta)|^2 \propto S(\theta) \ .$$

Below, these two quantities are used interchangeably, since the cross section calculation was ultimately normalized to the data. From this experimental determination of the angular dependence in the lab system, we can apply an accurate correction at fixed lab angles. This is necessary since each lab spectrum corresponds to a continuum of c.m. angles. For example at $\theta_{lab} = 6$ deg, for the range $E_{nn} = 0$ to 1.57 MeV, $\theta_{c.m.}$ goes from 12.52 deg to 12.85 deg. When $|g(\theta_{c.m.})|^2$ for different values of E_{nn} are compared (see Fig. 12), it is seen that there is no significant departure from the form of (8a). This fact demonstrates the validity of the Watson form in this angular region.

The angular dependence, $|g(\theta)|^2$, determined as described above, was then used to correct the 6 and 8 deg lab spectra. For the 6 deg and 8 deg spectra this dependence was approximated by a straight line, in the former case between values of $S(\theta)$ corresponding to 12.52 deg and 16.54 deg, c.m. These two points are obtained from (27) for $E_{nn} = .40$ MeV, $\theta_{lab} = 6$ deg and $\theta_{lab} = 8$ deg. This energy was chosen because it corresponded to the best statistical accuracy. Table II gives the values of $|g(\theta_{c.m.})|^2$ at 10 channel (0.342) intervals of the 6 deg spectrum. It should be noted that the maximum correction is about - 4%.

Table II. Values of $|g(\theta_{c.m.})|^2$ at 10 channel intervals.

θ_{lab} (deg)	E_{nn}	Channels from end point	$\theta_{c.m.}$ (deg)	$\lvert g(\theta)\rvert^2$	Error (%)
6	0	0	12.52	1.00	± 8
	.40	10	12.60	.9922	
	.79	20	12.68	.9833	
	1.18	30	12.77	.9740	
	1.57	40	12.85	.9645	

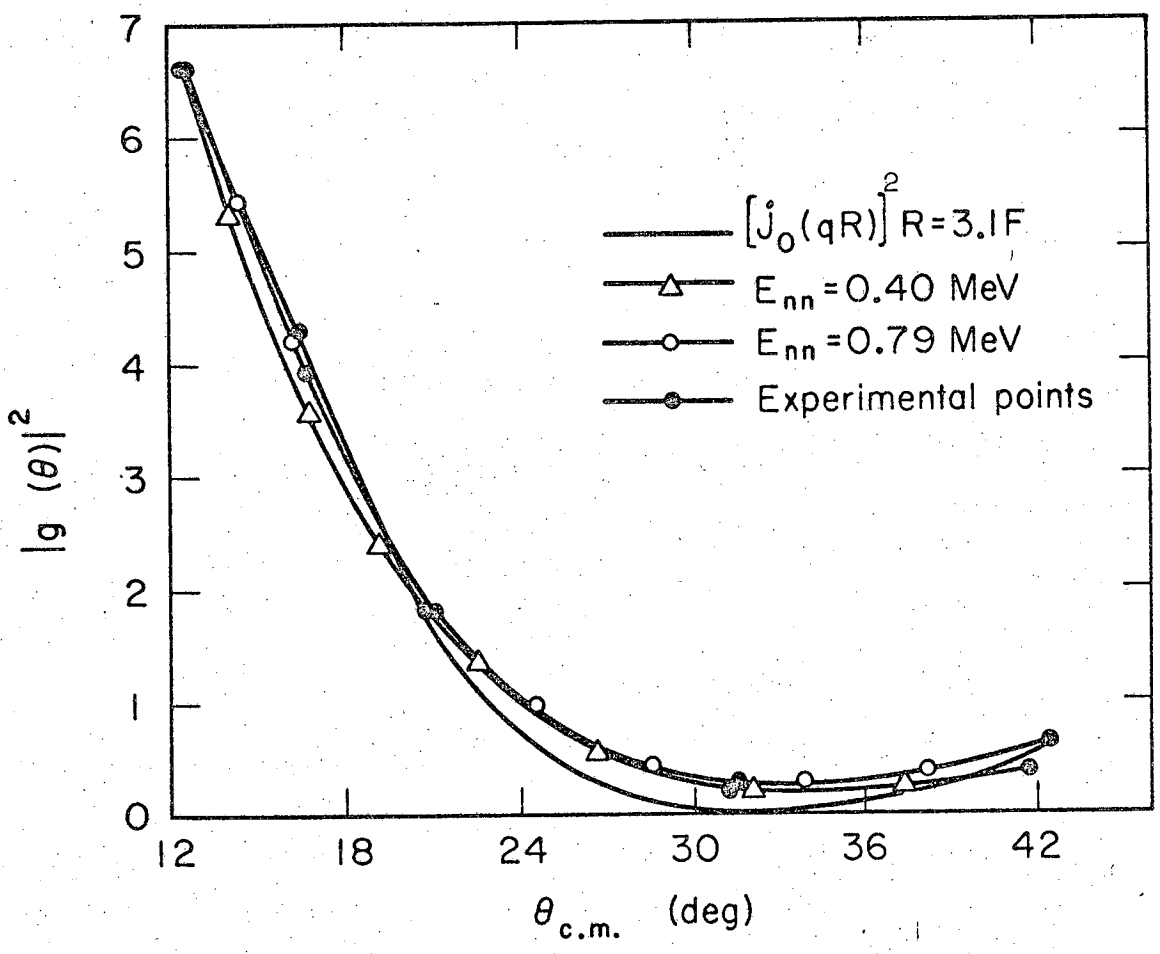

MUB-11206

Figure 12. Normalized functions of $|g(\theta)|^2$. See Sec. V.A for discussion of $[j_0(qR)]^2$.

4. Resolution Folding

The calculated function, $d^2\sigma/d\Omega dE$ must be combined with all sources of instrumental energy spread in order to simulate the observed spectrum. Since the energy spreading is the result of random processes, for a large number of events, we expect a monochromatic line to appear on the spectrum as a Gaussian distribution of energies. Therefore, the observed cross section can be expressed as

$$\sigma_R(E) = \int_{E_{min}}^{E_{max}} \sigma(E') \exp\left[-(E - E')^2/2(\Delta E)^2\right] \frac{dE'}{2\Delta E \quad 2\pi}, \qquad (28)$$

where

$$\sigma(E') = d^2\sigma/d\Omega dE\Big|_{E = E'} .$$

The quantity ΔE is the standard deviation of the Gaussian energy spread distribution. It was determined experimentally for He^3 from the width of the peak corresponding to the reaction $N^{14}(d,He^3)C^{13}$, with C^{13} in its ground state. These peaks are intrinsically monochromatic and therefore we may extract ΔE directly from their widths. Figure 13 shows the ground state peaks from which the half-widths were estimated. In principle one must correct for the additional kinematic energy spread of the $H^3(d,He^3)2n$ reaction in order to use the full width at half maximum (FWHM) of the C^{13} peak in (28). (This energy spread is due to the finite angular acceptance of the detector.) However, the energy spread of the He^3 from the $H^3(d,He^3)2n$ reaction is about 50 KeV compared to the 10 KeV of the $N^{14}(d,He^3)C^{13}$. The total spread estimated from Fig. 13 is 240 $\pm$ 14 KeV. Therefore the correction is negligible when folded in as an independent

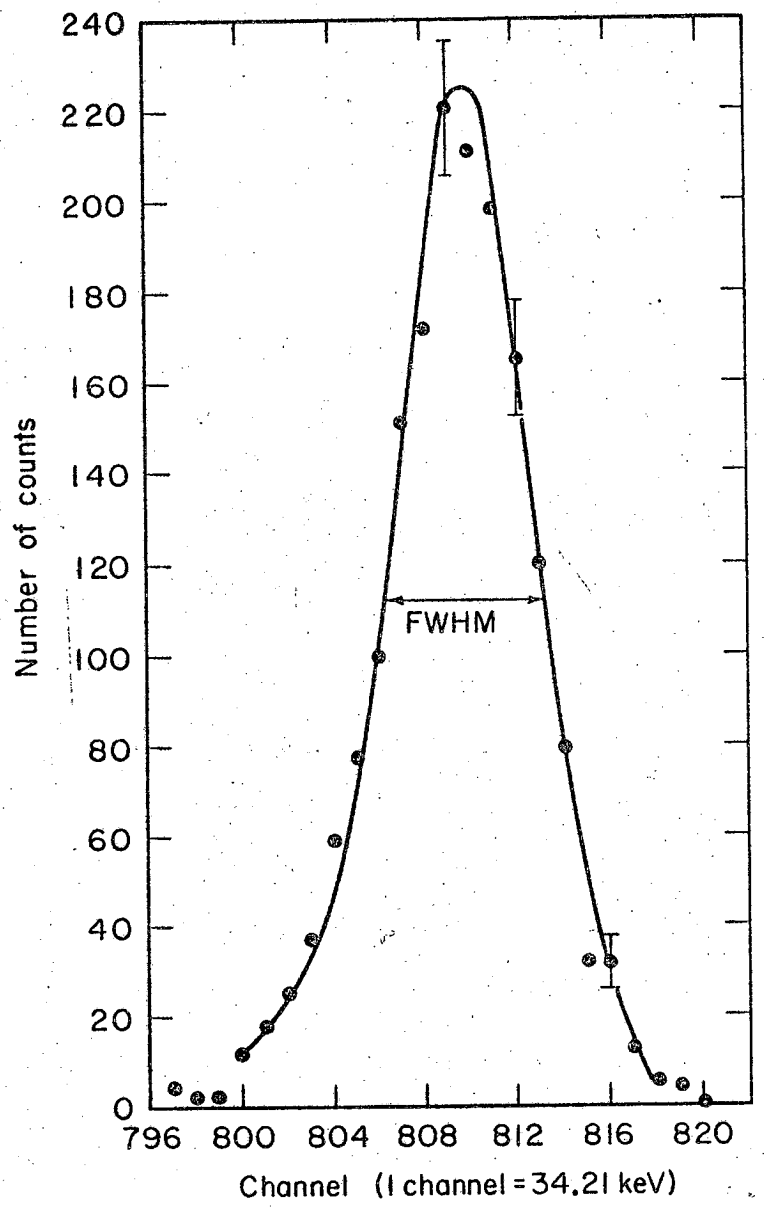

MUB-11211

Figure 13. Peak of ground state He^3 from $N^{14}(d,He^3)C^{13}$ at 6 deg.

random error.

The integral of (28) may be approximated by the sum

$$\sigma_R(E_j) = \frac{E_{max} - E_{min}}{N} \sum_{k=1}^{N} \sigma(E_K) \frac{\exp\left\{\left[-\left(E_K - E_j\right)^2 / 2(\Delta E)^2\right]\right\}}{2\Delta E\sqrt{2\pi}} \tag{29}$$

For simplicity, the indices in (29) are taken to correspond to channel energies in which the cross section is observed. (E_j is the lower edge of channel j.) Measurement of a cross section corresponds to averaging (29) over each instrumental channel width. Therefore,

$$\bar{\sigma}_R\left(E_j\right) = \sum_{k=1}^{N} \sigma\left(E_K\right) \int_{E_j}^{E_{j+1}} \exp\left\{\left[-\left(E_K - E'\right)^2 / 2(\Delta E)^2\right]\right\} dE' / 2\Delta E\sqrt{2\pi} \tag{30}$$

$$= \sum_{k} \sigma\left(E_k\right) \left\{- \mathrm{Erf}\left(E_j - E_k\right) + \mathrm{Erf}\left(E_{j=1} - E_k\right)\right\} .$$

Note that $\left(E_{max} - E_{min}\right)/N$, which is just the channel width, is cancelled by the averaging process. A simplification is obtained if we define

$$(\Delta\mathrm{Erf})_i = \mathrm{Erf}\left(E_j - E_k\right) + \mathrm{Erf}\left(E_{j=1} - E_k\right) \tag{31}$$

with

$$i = (j + 1) - k \qquad j \geq k \tag{31a}$$

$$i = k - j \qquad j < k .$$

Then

$$\bar{\sigma}_R\left(E_j\right) = \sum_{k,i} \sigma\left(E_k\right) \cdot (\Delta\mathrm{Erf})_i . \tag{32}$$

For the Gaussian function used in (30)

$$\sum_{i=1}^{11} (\Delta\mathrm{Erf})_i = .9998 .$$

Therefore, the maximum value of i, used in (32) was 11. A computer program was used to generate the 11 × 50 matrix of (32) for each value of a_{nn}.

B. Results and Errors

1. χ^2 Distribution and Errors

After calculating (26) and folding into it the resolution loss by using (32), the next step is to compare the calculation with experimental data by calculating the χ^2 distribution as a function of a_{nn}. All the calculations have been done at energy intervals corresponding to the observed channels, and we may readily form the sum

$$\chi_a^2 = \sum_{i=1}^{N} \left(Y'_{i,a} - X_i\right)^2 / Y'_{i,a} \quad . \tag{33}$$

Here, $Y'_{i,a}$ is the calculated cross section for a particular value of a_{nn}; X_i is the observed cross section. Since we are concerned with the shape of the spectrum, there is no need of calculating absolute cross sections, and some reliable criterion for the normalization of the calculated cross sections is necessary. The factor chosen was one obtained by requiring χ^2 to be a minimum.

If

$$Y'_{i,a} = K\, Y_{i,a}$$

where $Y_{i,a}$ is any unnormalized calculation, then for

$$K = \left[\left(\sum_i \left(X_i^2 / Y_{i,a}\right)\right) / \sum_i Y_{i,a}\right]^{1/2}$$

χ^2 is a minimum. Figures 14, 15, and 16 show these appropriately normalized calculations superposed on the experimental spectra. While the two fits

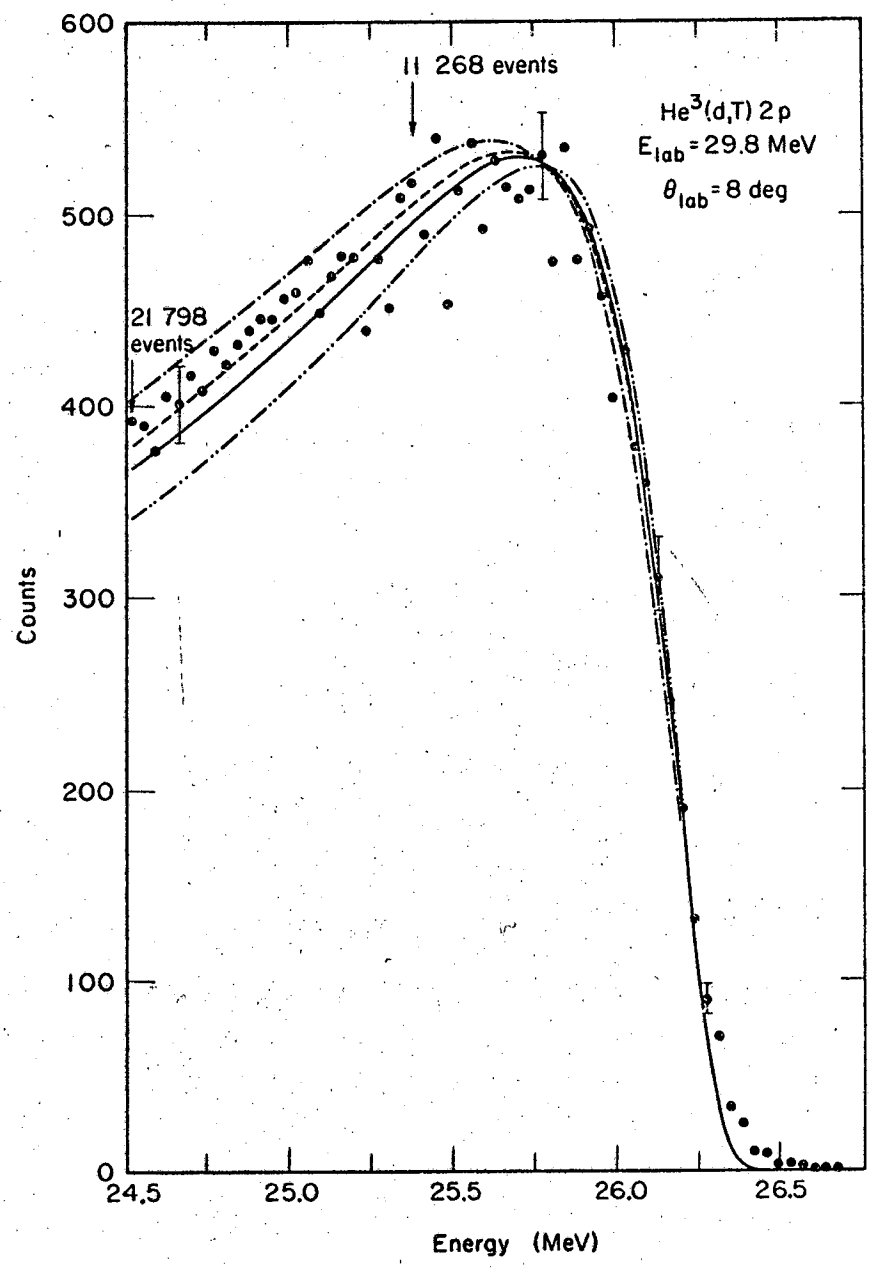

MUB-8714

Figure 14. Triton spectrum at 8 deg lab of the reaction $He^3(d,t)2p$ at 29.8 MeV with theoretical fits calculated for 11 268 events and for 21 798 events. The dots are experimental points. The solid line is the best fit for 11 268 events with a_{pp} = - 7.69 F. The dashed line is the best fit for 21 798 events with a_{pp} = - 7.41 F. The dash-dot line is obtained with a_{pp} = - 6.90 F, for 11 268 events, and the dash-double dot line is obtained with a_{pp} = - 8.33 F; they indicate the sensitivity of the theoretical curve to variation of a_{pp}.

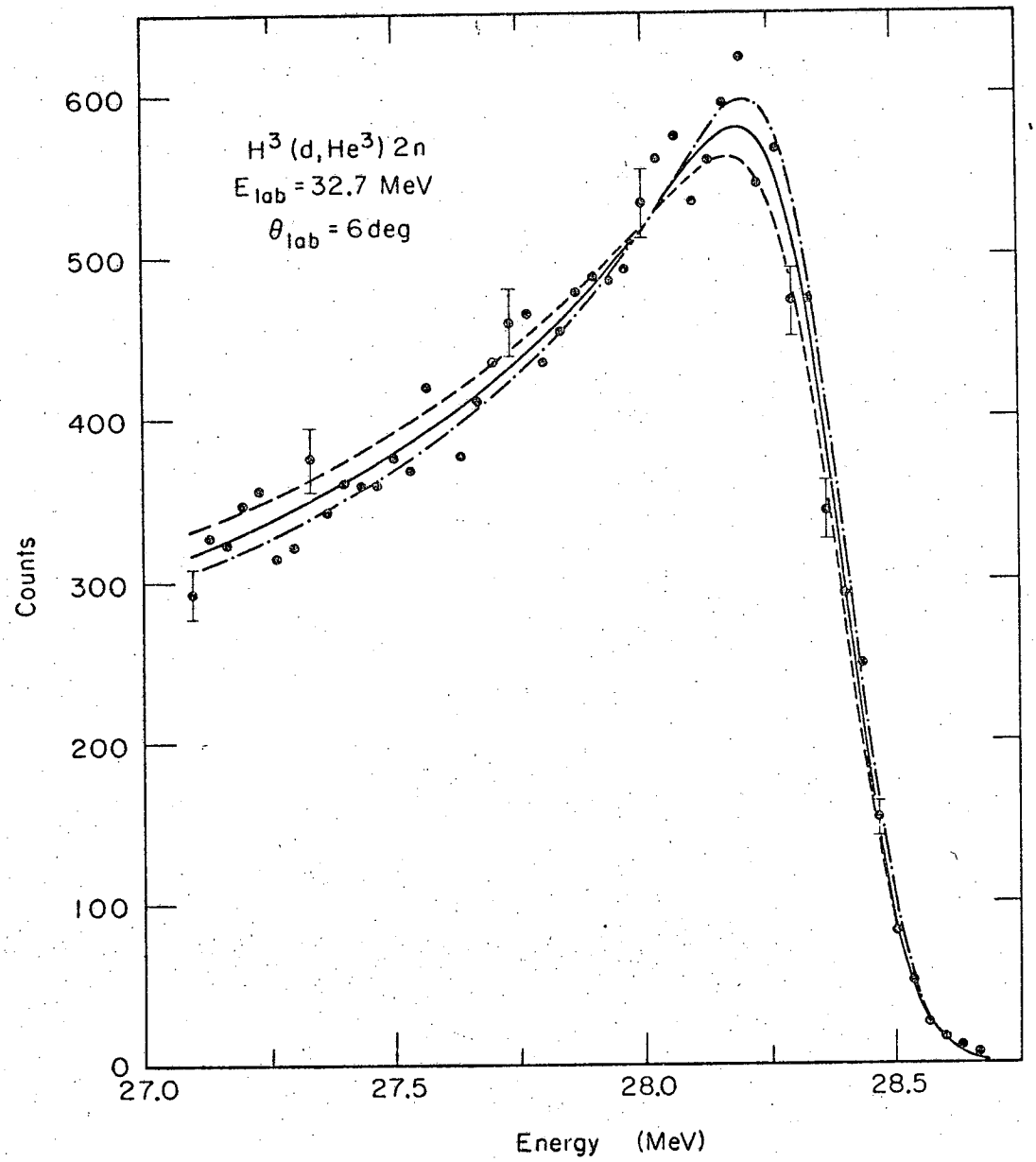

MUB-8712

Figure 15. He^3 spectrum at 6 deg lab of the reaction $T(d,He^3)2n$ at 32.7 MeV with theoretical fits calculated for 17 782 events. The solid line is the best fit for $a_{nn} = -16.1$ F. The dashed line is obtained with $a_{nn} = -14.0$ F and the dash-dot line corresponds to $a_{nn} = -18.0$ F.

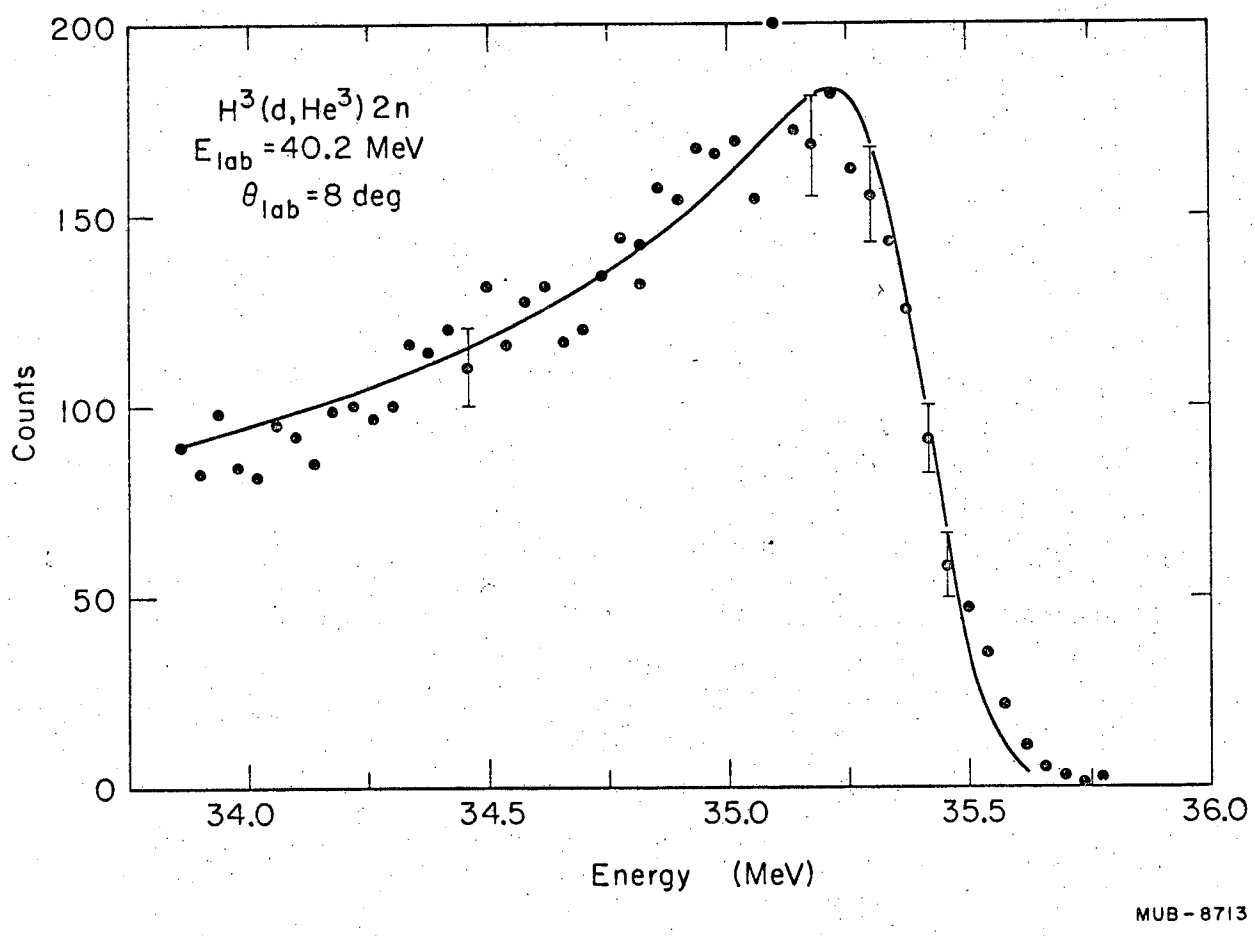

Figure 16. He^3 spectrum at 8 deg lab of the reaction $T(d,He^3)2n$ at 40.2 MeV together with the curve calculated for a_{nn} = - 16.0 F. It is consistent with the value determined at 32.7 MeV.

at 8 deg appear to be quite good, there is unfortunately some background from the reaction $d + He^3 \rightarrow n + p + He^3$ evident at the high energy end of the spectra. At 6 deg, this background was negligible and the fits show remarkable stability over the full range of energy which is covered by 46 channels or data points. This can be seen in Table III (each "point" in this table corresponds to an observed channel width). Therefore, it was from this spectrum that the value of a_{nn} was extracted. The values of χ^2 as a function of a_{nn} are shown in Fig. 17. Each point in this distribution corresponds to the sum (33) over 46 data points. A parabola was fitted to the 8 values of χ^2 between $a_{nn} = -15.25F$ and $a_{nn} = 17.0F$. The equation of this parabola was

$$Y_i = \left(\chi_i^2 - 45.0\right) = 4.8257 - 9.1705\, x_i + 5.6559\, x_i^2 \qquad (34)$$

where

$$x_i = -\left(a_{nn}\right) - 15.25 \text{ in fermis.}$$

Table III. Stability of χ^2

θ_L (deg)	Points (Channels)	Number of points	Minimum a_{nn}(f)	χ^2
6	1 - 46	46	16.1	46.1
(32.7 MeV)	5 - 46	42	16.4	43.4
	16 - 46	31	16.4	25.8
8	8 - 46	39	16.0	38.9
(32.7 MeV)	16 - 46	31	16.2	33.9
8	5 - 46	42	15.7	30.6
(40.4 MeV)	16 - 46	31	16.8	19.4

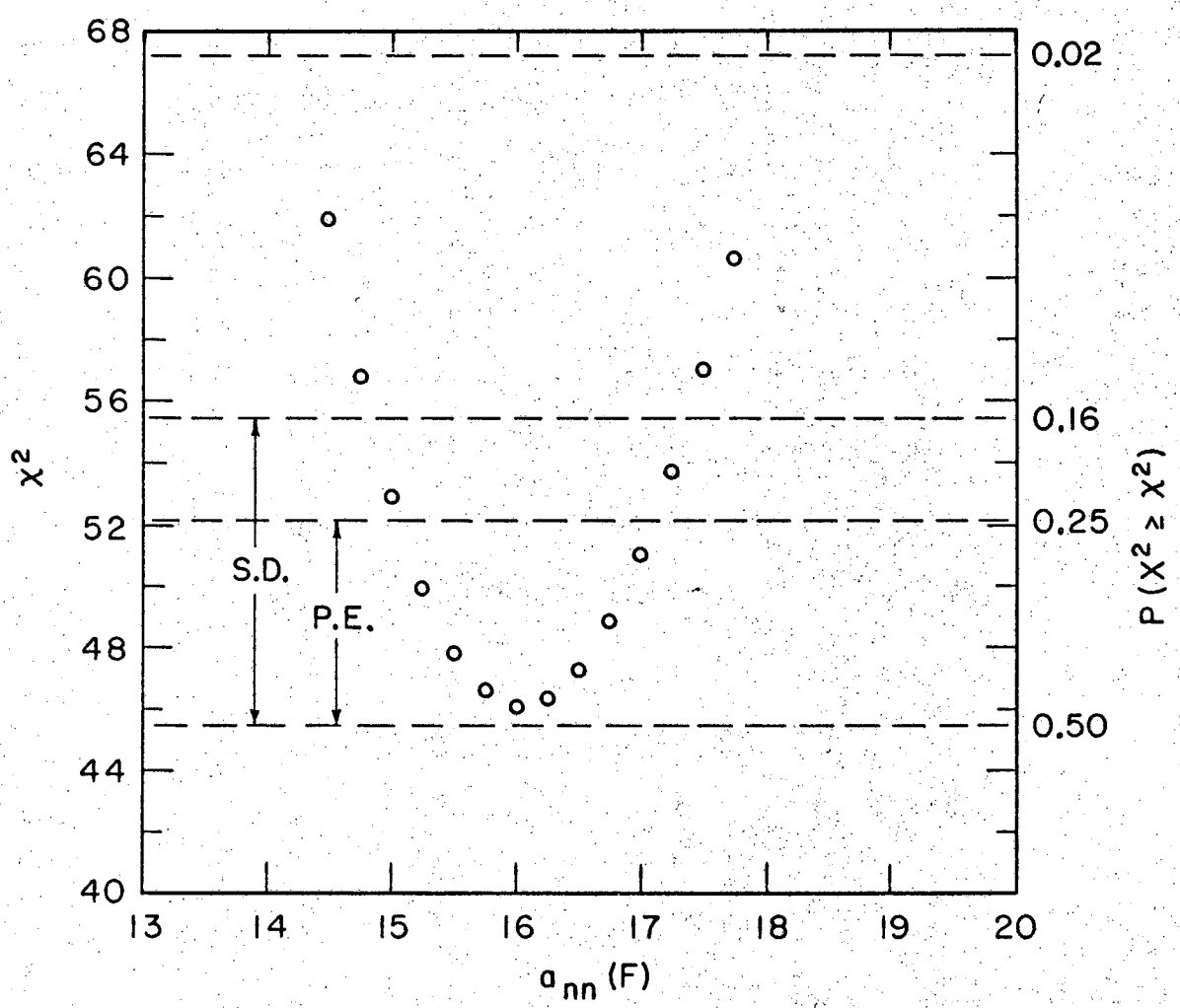

MUB-11212

Figure 17. Values of χ^2 as a function of a_{nn} for fit of θ = 6 deg. E_d = 32.7 MeV spectrum.

The least-squares solutions for the coefficients of Eq. (34) are linear in the Y_i's. Therefore the standard deviation of these coefficients is readily obtained from the standard deviations of the calculated Y_i's, which are

$$S_3 = \left\{ \sum_{i=1}^{n} \left(Y_i - Y_{i,c}\right)^2 \Big/ (n - 3) \right\}^{1/2}$$

where $Y_{i,c}$ is the calculated value from Eq. (32). If we write

$$Y_i = c_0 + c_1 x_i + c_2 x_i^2$$

then the minimum χ^2 corresponds to

$$Y_{min} = - c_1/2c_2 \ .$$

The uncertainty in the position of this minimum is then taken as the sum of the percentage standard deviations. In Eq. (34), this is equal to $\pm$ .03F, which is certainly negligible. The minimum χ^2 corresponded to

$$a_{nn} = - 16.06F.$$

2. Standard Deviation and Probable Error of a_{nn}

The number of data points, N in the sum, Eq. (36), is equal to 46; this corresponds to 45 deg of freedom and we may use the asymptotic form for the χ^2 distribution. For $\nu > 30$, where ν is the number of degrees of freedom, the quantity $\sqrt{2\chi^2} - \sqrt{2\nu - 1}$ is distributed normally. Therefore, the value of χ^2 corresponding to the mean of this distribution for 45 degrees of freedom is 44.5. Similarly, the value of χ^2 corresponding to one standard deviation above the mean is 55.540, and the probable error corresponds to $\chi^2 = 52.162$. As can be seen from Fig. 17, the minimum χ^2, 46.095, is very near the mean χ^2 and hence there is no ambiguity in the definition of the error associated with the determination of the scattering length. Thus the probable error and standard deviation were

obtained by finding the intersections of these values of χ^2 with the parabola of Eq. (34). The following values were obtained (see Fig. 17):

$$P.\ E. = \pm\ 1.04\ F$$

$$S.\ D. = \pm\ 1.29\ F.$$

C. Experimental Errors

A most convenient and reliable method of obtaining the effect of experimental uncertainties on the value of the scattering length is simply to substitute input values corresponding to the limits of error into the calculations. This procedure was used for the beam energy, channel width, $g(\theta)$, and the Gaussian FWHM of the resolution loss. The resulting χ^2 distributions are shown in Fig. 18 and are discussed below.

1. Detector Angle and Target Pressure

These two quantities, although they are primary measurements made in the course of the experiment, do not enter into the expressions for the observed cross section, Eq. (26). However, these uncertainties propagate into the quantities which do serve as the input parameters for the calculation.

In the determination of detector angle there were three main sources of error. First, the positioning of zero-deg calibration of the detector-arm vernier scale was accomplished by optically aligning the center of the entrance collimator and the center of rotation of the counter arm (also the target center) with the center of the counter collimator. The centering of these collimators was accurate to about ± .005 in. and they were, respectively, 18 and 12 inches from the center of rotation. The uncertainty in the zero deg position of the detector arm is therefore, ± .01 deg.

The estimated uncertainty in the determination of the beam center

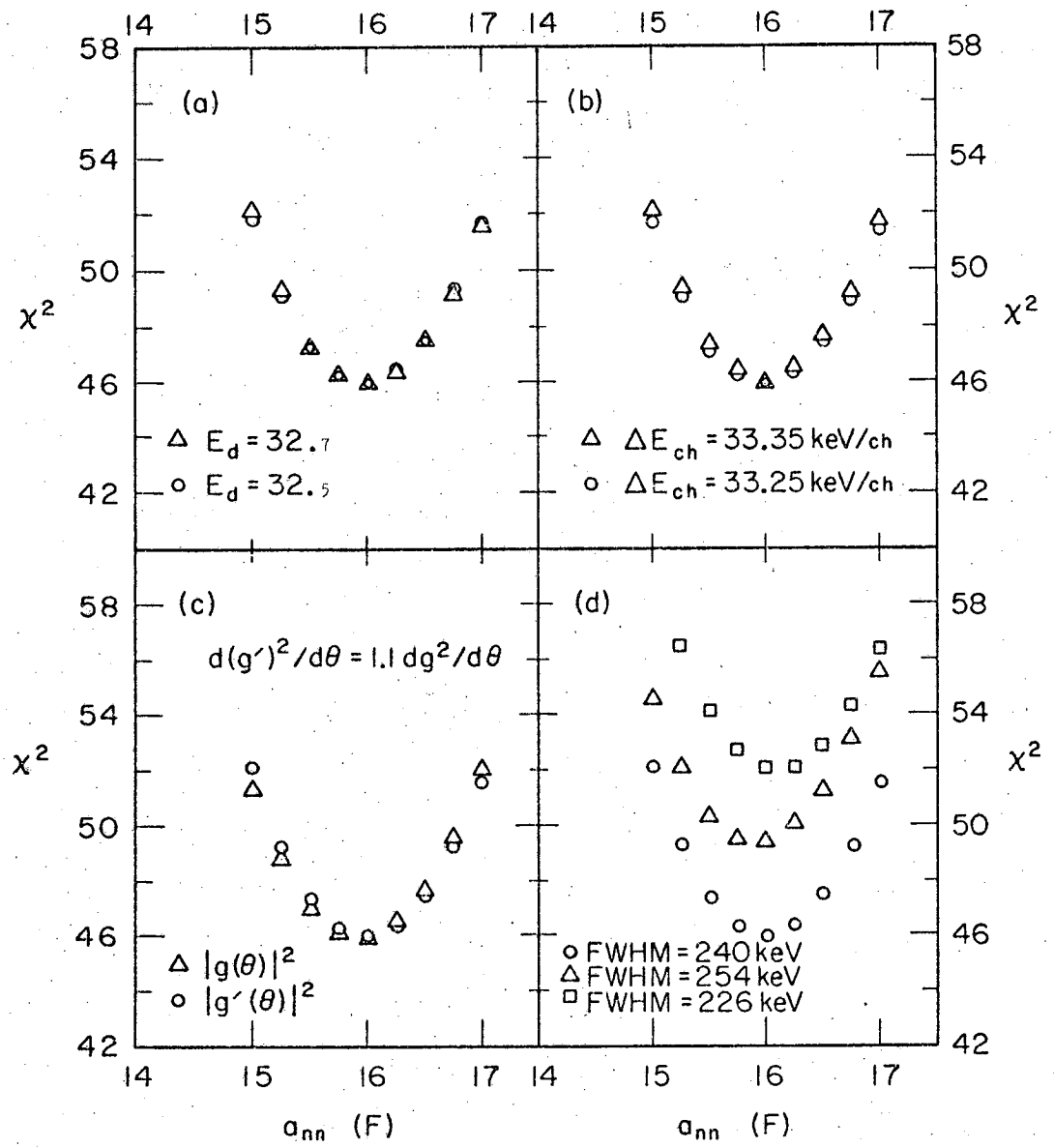

Figure 18. χ^2 vs. a_{nn} for (a) variation of incident energy, (b) variation in channel width, (c) variation in slope of $|g(\theta)|^2$, (d) variation in FWHM.

from the beam profiles (see Fig. 2) was ± .03 deg.

The reading error of the detector-arm vernier scale was ± .03 deg. Therefore the total angular uncertainty is approximately ± 0.04 deg.

Since absolute cross sections were not being measured, pressures were determined by means of compound gauges on the filling system, or in the case of the tritium target, on the target chamber itself. We estimate the total error on these gauges to be, at worst, about ± 10%. This uncertainty becomes an uncertainty of the energy losses in the target gas, but ultimately has no effect whatsoever on the scattering length determination, as will be shown below.

2. Beam Energy Determination

The uncertainty in the thickness of the aluminum absorbers used for the range-energy measurement was ± 0.2%. (Since there was a short air gap between the absorbers and the Faraday cup in which the beam was collected, there is an additional uncertainty in the total range due to the rather low energy (~ 6 MeV) which the particles have when they reach this gap. This error was estimated to be ± 0.2% of the total range. The uncertainty in the determination of the mean range is estimated to be 0.1% (see Fig. 6). As indicated above, there are additional uncertainties in target center energies, due to uncertainties in target pressures, but these are quite small (± 8 KeV in the largest case, the nitrogen target). The total range was found to be 805 ± 5 mg/cm^2 of aluminum corresponding to an energy of 32.69 ± .13 MeV. Figure 18a shows the two χ^2 distributions resulting from the calculations with E_d = 32.7 and 32.5 MeV. The latter energy would correspond to an error of - .2 MeV. However, as is evident, there is no significant shift in the minimum of the χ^2 distribution.

3. Channel Energy Width

The energy separation observed in the lab for reactions ending in different nuclear levels depends on beam energy and detection angle through kinematics. The uncertainties in separation were obtained simply by calculating the kinematics for all levels in 0.1000 MeV beam energy intervals, and 1 deg angular intervals. Sample errors, δE, found in this way for the four levels used to obtain the channel width are shown in Table IV. The uncertainty δ(ch) is the estimated error in the positions of the peaks corresponding to each level. As can be seen in the table, these errors are quite small. Figure 18b shows the χ^2 distribution corresponding to the mean value of the target center channel width, 33.25 KeV/channel, and to a channel width .10 KeV/channel greater. There is no significant shift in the minimum of the χ^2 distribution. The value in

Table IV. Sample errors for channel energy width.

Level	Lab angle (deg)	Separation (from ground state) Channels	Energy (MeV)	Errors δE	δ(ch)	Channel width (KeV/chan.)
7.55	6	226.3	7.750	± .001	± .2	34.25
	8	226.1	7.747			34.26
	20	225.3	7.695			34.15
3.09	20	90.6	3.100			34.22
8.85	6	267.6	9.132			34.13
	8	267.0	9.128			34.19
6.87	20	203.7	6.985			34.29
				Average		34.21 ± .08 (max. dev.)
				Calibrated pulser		34.38 ± 1%

Table IV differs from 33.25 since it is not corrected to the target center.

4. Angular Dependence - $|g(\theta)|^2$

The major uncertainties in the linear approximation for $|g(\theta)|^2$ are due to the statistical errors of the events used and the uncertainty in the difference of the angles used. This factor, as applied to the 6 deg spectrum was obtained from the ratios of cross sections of the 6 and 8 deg spectra. The error in the slope is about ± 11% (see Fig. 12). Figure 18c shows two χ^2 distributions; one for the central value of $|g(\theta)|^2$ as observed, and one for a value whose slope is 10% greater. The shift in the minimum is less than 0.1 F.

5. Energy Resolution

The uncertainty in the full-width at half-maximum (FWHM) of He^3 corresponding to the ground state of C^{13} was ± 0.4 channel (13.7 KeV). This error is the result of estimating the FWHM instead of doing a detailed fit of a Gaussian shape to the peak. However, in practice, we are doing such a detailed fit to the high-energy end of the $H^3(d,He^3)2n$ spectrum. This is so because the "true" spectrum, i.e. the cross section before resolution loss is folded in, rises from zero at the maximum energy to its peak value in only 120 KeV (3.5 channels). Since in (28) we assume that the "true" particle energies appear as the mean values of Gaussian distributions, all events above the maximum energy are really the Gaussian tail of the nearly monochromatic peak of the spectrum. Therefore the χ^2 fit in this region will primarily be a fit to the FWHM of the Gaussian used in (30). In the light of these considerations, the results of varying the FWHM are very gratifying. In Figure 18d are shown the three χ^2 distributions corresponding to the value of the Gaussian FWHM and its uncertainty, 0.240 ± .014 MeV. (See Fig. 13.) There is a large increase in the minimum value of χ^2 for each of the extreme values of the FWHM. This increase is

entirely in the 15 highest (energy) points, i.e. the Gaussian tail. For these points χ^2 goes from its minimum of 19.7 at FWHM = 0.240 MeV to 23.1 at FWHM = 0.254 MeV and 26.0 at FWHM = 0.226 MeV. On this basis we can say that the value used is very near a best fit to the data, and the large change in χ^2 for the quoted uncertainty indicates a much smaller probable error. Nevertheless, even for these rather over-large uncertainties the shift in the minimum is only about ± 0.1 F. Therefore, the actual resulting probable error in the scattering length is considerably less and can be neglected.

V. DISCUSSION

A. Long Range and Short Range Production

It has been previously pointed out that for small angles, the reaction $He^3(d,t)2p$ is a direct reaction of the "pick-up" type.[22,23] The angular distributions obtained for the reaction $H^3(d,He^3)2n$ indicate that it too, as would be expected, proceeds by the pick-up mechanism at small angles. At sufficiently high energies, the angular distributions for such reactions are qualitatively well predicted by simple plane wave Born approximations for the transition matrix;[24] in these approximations it is assumed that the production potential, V, is very short range. Indeed, it is possible to get fits to the angular distributions by assuming V to be a delta-function in the coordinates of the incident particle and "picked-up" nucleon. In the above cases, this nucleon is in an $\ell = 0$ state initially, and the crude delta-function model gives

$$d\sigma/d\Omega \propto \left[j_o(qR)\right]^2$$

where q is the momentum transfer and R is the reaction radius.

In Fig. 11 there are shown the plots of $(d\sigma/d\Omega)$ at constant E_{nn} for $H^3(d,He^3)2n$ reaction at $E_{nn} = 0.40$, 0.79 and 1.57 MeV. It should be noted that their relative magnitudes at a fixed θ are determined by the enhancement at each value of E_{nn}. Figure 12 shows two of these same curves normalized to the value of $|g(\theta)|^2$ for $E_{nn} = .140$ at 12.52 deg. The slope of the curves between 12.52 deg and 21.31 deg is quite uniform, demonstrating that the factorization into angular dependence and energy dependence at small angles is a good and reliable method of treating the spectra. Also shown in Fig. 12 is $\left[j_o(QR)\right]^2$, R = 3.1 F. At small angles its slope and general shape agrees well with the observed $|g(\theta)|^2$ which

demonstrates the validity of the direct reaction model.

Direct reactions of this kind, which are highly localized in space, in contrast with other conceivable mechanisms producing the same final state, are best suited to the momentum dependence separation which leads to expression (8a). Quoting Watson:[1] "for processes...for which the range of V is considerably less than the range of v there should be no serious modification of v since the effect of the final state interaction comes from regions of space for which V = 0." (Here v is the final state interaction, and V is the production interaction.) In the case of $He^3(d,t)2p$ this spatial separation of primary and final-state interactions, characteristic of direct reactions, can readily be seen in the Born approximation transition matrix for the process.[23]

$$M = \int \exp\left[i\left(\vec{Q} \cdot \vec{z}\right)\right] u'\left(\vec{z}\right) d^3z \int u\left(\vec{x}\right) \chi_q^{(-)*}\left(\vec{x}\right) d^3x$$
$$\int \exp\left[-i\left(\vec{Q}' \cdot \vec{y}\right)\right] u'\left(\vec{y}\right) d^3y \int \phi_d\left(\vec{r}\right) u\left(\vec{r}\right) V\left(\left|\vec{y} - \frac{1}{2}\vec{r}\right|\right) d^3r \qquad (35)$$
$$\left\langle S_{H^3}(4,5,3) S_{pp}(1,2) \middle| P(\sigma,T) \middle| S_{He^3}(1,2,3) S_d(4,5) \right\rangle .$$

The three-body wave functions of H^3 and He^3 were assumed separable in the form

$$\psi(1,2,3) = Nu\left(\vec{r}_1 - \vec{r}_2\right) u'\left(\vec{r}_3 - \frac{1}{2}\left[\vec{r}_1 + \vec{r}_2\right]\right). \qquad (36)$$

The S's are appropriately symmetrized spin-isospin wavefunctions and $P(\sigma,t)$ represents the spin dependent part of V, the primary interaction. The spatial and momentum coordinates of (35) are defined as:

$$\vec{r} = \vec{r}_4 - \vec{r}_5 \qquad \vec{Q} = \frac{2}{3}\vec{K} - \vec{k}$$
$$\vec{x} = \vec{r}_1 - \vec{r}_2 \qquad \vec{Q}' = \vec{K} - \frac{2}{3}\vec{k}$$

$$\vec{y} = \vec{r}_3 - \frac{1}{2}\left(\vec{r}_4 + \vec{r}_5\right) \qquad \vec{q} = \left(\vec{k}_1 - \vec{k}_2\right)/2$$

$$\vec{z} = \vec{r}_3 - \frac{1}{2}\left(\vec{r}_1 + \vec{r}_2\right)$$

$\vec{K}$ and $\vec{k}$ are the incident and final momenta respectively, in the c.m. system.

In this direct reaction model, the production potential is just an interaction between nucleons 3 and 4. It is quite evident that this production process is independent of the relative momentum and separation of nucleons 1 and 2, the two-proton system. Therefore the production process does not distort the momentum dependence on q in (35), which is contained in the factor

$$\int u(x)\chi_q^{(-)*}(x)d^3x \quad . \tag{37}$$

In Sec. II. A. it was shown that a necessary condition for the simple factorization of the momentum dependence of (4), $\left(\frac{1}{q}\right)\sin\delta\,(q)$, is that $qr \ll 1$. At $r = 0$ this factorization is an exact procedure for the asymptotic wave function. (The Jost function enhancement is also obtained at $r = 0$.) Hence, the use of $\left(\frac{1}{q}\right)\sin\delta$ as an enhancement may be said to correspond to short range production processes. If this short range condition is not fulfilled, then the factorization cannot be done and the integrals (5) and (37) depend on the detailed behavior of $g_q^-(r)$ in (3) or $\chi_q^-(r)$ in (37). Furthermore, the matrix elements also depend on the form of $\chi_a^{(+)}$, which is not, in general well known. Even in using the Born approximation, there is, generally, a considerable uncertainty in the unperturbed form of $\chi_a^{(+)}$. This is the case with u(x) of (37), the wave function of the two protons in the He^3 nucleus.

A good example of these considerations is nucleon-deuteron breakup reaction, from which attempts have been made to extract the neutron-neutron

scattering length.[25,26] In the impulse approximation, the dependence on q, the relative momentum of the two like nucleons is contained in the matrix element for forward scattering of the odd nucleon[26,27]

$$T = T_o(\vec{K}) \int d^3r \, \chi_q^{(-)*}(r) \phi_d(r) \exp\left[i\vec{K} \cdot \vec{r}/2 \right] \tag{38}$$

where $\vec{K}$ is the momentum transfer, and $\phi_d(r)$ is the deuteron wave function. Using the Hulthen function, R. J. N. Philips calculated (38) and pointed out considerable departure from the factored form of (8). Appropriately, Phillips called the nucleon-deuteron break-up a "long-range" process, since the production of the final state takes place over the range of non-zero values of the deuteron wave-function, which being relatively extensive, makes necessary consideration of values of $qr \approx 1$ for E_{np}, $E_{nn} \geq 1$ MeV. The net effect of this "overlap" is to give a more narrowly peaked spectrum. Therefore, if one attempts to fit the spectrum with the Watson form or some other short-range approximation, the scattering length obtained will be too large. Indeed the scattering lengths obtained from experiments utilizing $n + d \rightarrow n + n + p$ range from - 21.6 F (no error quoted) by Cerineo et al.[25] to $-23.6 \begin{smallmatrix} +2.0 \\ -1.6 \end{smallmatrix}$ F by Voitovetski et al.[26] In the light of later work, these values seem definitely to be several fermis too large. However, in carefully evaluating the expression (38) as it occurs in the transition matrix for $\pi^- + d \rightarrow n + n + \gamma$, McVoy[3] showed that for q corresponding to $E_{nn} < .8$ MeV, the momentum dependence of (38) could be represented as $\sin \delta/q$ to within about 2%. (However he estimates that the discrepancy due to the d-wave component of the deuteron may be as high as 4%.)

Therefore, we can say that the distinction between "long-range" and "short range" production is a most important criterion in applying the

Watson form; the factorization is valid only within a limited region of low particle-pair relative energies. This energy region is defined by the range of the production process. Consider specifically the d + T and d + He^3 reactions. Using a Gaussian wave function[29] in (36) we find the average separation of a nucleon pair in the He^3 nucleus to be

$$< r_{12} >_{He^3} = 1.29 \text{ F},$$

compared to the deuteron for which

$$< r_{12} >_{deut} = 3.26 \text{ F},$$

using the Hulthen wave function. Therefore in the range of energies we have considered, $E_{nn} < 1.57$ MeV, assuming the same $< r_{12} >$ for H^3 as for He^3 we find

$$q < r_{12} >_{H_3} < .25 ,$$

and the short range approximation is valid.

If it is possible to use the factorization (4) one avoids the necessity of explicit evaluation of the production matrix element, which generally depends on too many uncertain quantities. Such evaluation has often been done using the Born approximation, a highly dubious procedure for low energies, aside from the fact that the form of the spectrum may depend critically on the form of the initial state two-nucleon wave function, as stated above. This effect is illustrated in Fig. 19 in which is plotted the "overlap integral," (38), for neutron-deuteron breakup, with subsequent final state interaction of the two neutrons, and the "short-range" approximation, i.e. essentially the Watson form, both calculated by Phillips.[28] It is readily seen that the effect of the "long-range" production is to

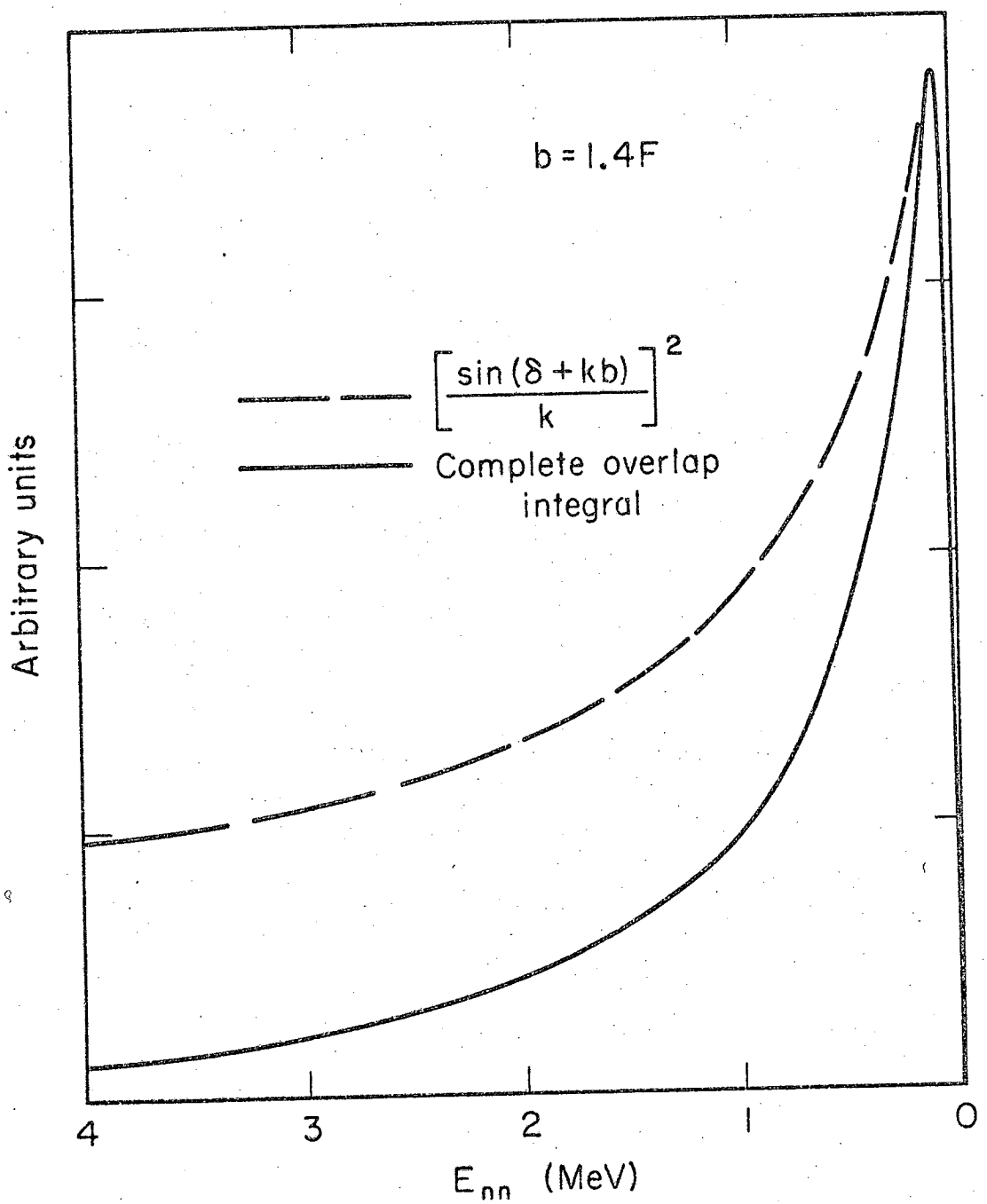

MUB-11207

Figure 19. Odd nucleon spectrum of nucleon-deuteron exchange with and without short-range approximation.

favor small values of E_{nn} more than in the case of short range production, thus narrowing the resulting peak.

A similar effect seems to be present in the reactions $H^3(n,d)2n$ and $He^3(p,d)2p$, but the exploration in terms of long range production is rather obscure in view of the fact that the Watson form gives such excellent results for the reactions $He^3(d,t)2p$ and $H^3(d,He^3)2n$. Ajdacic et al.[30] investigated the $H^3(n,d)2n$ reaction at 14.4 MeV, and attempted to extract a_{nn} from their data. They found that the peak at the high-energy end of the deuteron spectrum, corresponding to small E_{nn}, was much narrower than the prediction of the Watson form. They used the Born approximation to extract the value $a_{nn} = -18 \pm 3$ F, and as explained earlier this is questionable.

On the other hand, Tombrello and Bacher,[30] investigating the mirror reaction $He^3(p,d)2p$ at 11.94 MeV, also found a much narrower peak than could be described by the Watson form for the proton-proton interaction, but they fitted their data by assuming an additional interaction. It was assumed that this interaction took place between the deuteron and the p-p system considered as a single particle, and by utilizing only Coulomb and centrifugal effects a best fit to the data was obtained if this interaction was present in an $L = 3$ state. However, this description ignores an essential feature of three-body kinematics that only one pair of particles may have zero or low relative momentum in a given configuration. Thus the customary treatment[10] of multiple final state interactions considers the total enhancement as the product of enhancements due to the interaction of each pair of particles in the three particle system. It is kinematically impossible for the two protons to have low relative momentum at the same time that the deuteron has low momentum relative to the c.m. of the two

protons. However, the deuteron and one proton may have zero relative momentum, but the deuteron then must have large momentum relative to the second proton; this occurs at $E_d = 1/4\ E_d^{max}$. For non-resonant attractive potentials, the final state pair enhancement always peaks near zero relative momentum for the pair. Hence we expect to see the effects of the p-p interaction at the upper end of the deuteron spectrum, while the p-d interaction should appear at low energy. Thus the residual effect of the p-d interaction could only appear, if it does at all, as a broadening of the proton-proton peak at high energies, rather than the observed narrowing.

B. Correlation Experiments

The reaction $He^3 + d \rightarrow p + p + t$ has been studied extensively by means of correlation experiments in which two of the final-state particles are detected in coincidence.[32,33] If, for some reason, it is desired to determine all three momenta in the final-state then such an experiment is necessary, since any linearly independent combination of three angles and/or energies is required in the c.m. system. However, it is only necessary to measure the momentum of a single particle in order to determine the relative energy of the other pair, which is certainly the most relevant quantity in describing the pair interactions. For example, E_{pp}, the energy of the two protons in their own c.m. system, is the only experimental parameter necessary to describe completely s-wave nucleon scattering (which includes the positions of resonant states, if any). The relative energy of particles 1 and 2 is

$$E_{12} = E_0 - (m_1 + m_2 + m_3)E_3/(m_1 + m_2), \tag{39}$$

where E_3 is the energy of the third (observed) particle in the c.m. system,

and E_0 is the total energy. For the specific case of $He^3 + d \rightarrow p + p + t$ we have

$$E_{pp} = E_0 - 5/2\ E_3\ ,$$

where E_3 is the triton energy. The advantages of a single detector experiment are well illustrated by the Dalitz triangle for this reaction, shown in Fig. 20. The inset at the left of the figure shows the spectrum $\frac{d^2\sigma}{d\Omega dE_3}$ in the c.m. system, which is seen to be the projection of all events, at a fixed c.m. angle for the triton, on to the E_3 (triton energy) axis. We see from (39) and the Dalitz triangle that in observing such a spectrum, from E_3 equal to zero to its maximum value, 2/5 E_0, we are covering the complete range of E_{pp} and summing over all other kinematic parameters. Each value of E_3 corresponds to a straight line of constant E_{12} on the plot; the spectrum of E_3 then corresponds to the entire area of the plot. On the other hand, in a correlation experiment, a fixed particle energy corresponds to one or two points on the Dalitz plot, and the locus of the spectrum of particle energies is generally a rather complicated curve, which intersects the lines of constant E_{12} at a point. Therefore the obvious advantage of the single detector experiment, besides its simplicity, is that it measures all events of a given E_{12} at a fixed detector angle, rather than the small fraction obtainable through the correlation experiment. This is reflected of course by much higher counting rates.

Regions of low relative momentum for each pair are shown as shaded regions on the plot. It can be seen that for any energy spectrum, regions of minimum relative energy cannot overlap and separation of enhancements depends on E_0, the total c.m. energy.

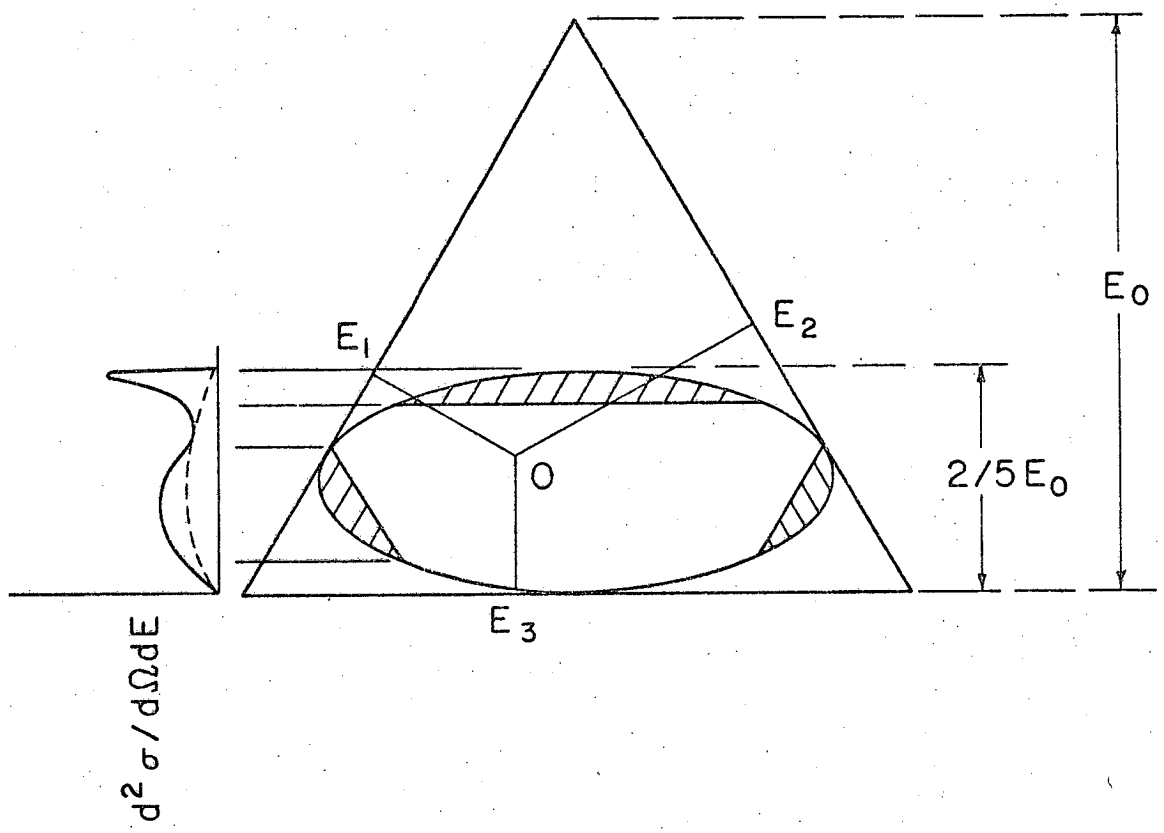

MUB-11208

Figure 20. Dalitz triangle and projection for $He^3(d,H^3)2p$.

C. The Reaction $He^3(d,t)2p$

There is very strong evidence for the validity of final state interaction theory in determining the neutron-neutron scattering length from the reaction $He^3(d,t)2p$. Spectra from the reaction $He^3(d,t)2p$ were obtained using 29.8 MeV deuterons under identical experimental conditions.[35] The reaction $N^{14}(d,t)N^{13}$ was used to determine the energy scale and resolution. The proton-proton scattering length was extracted from these spectra by using (23). Shown in Fig. 14 is the spectrum at $\theta_L = 8$ deg and the theoretical fit. For 21,798 events ($E_{pp} = 0$ to 2.38 MeV)

$$a_{pp} = -7.41 \begin{smallmatrix} +.39 \\ -.49 \end{smallmatrix} \text{ F.}$$

For 11,268 events ($E_{pp} = 0$ to 1.58 MeV) the scattering length is

$$a_{pp} = -7.69 \begin{smallmatrix} +0.61 \\ -0.67 \end{smallmatrix} \text{ F.}$$

The errors are probable errors determined from asymmetric χ^2 distributions. The accepted value of a_{pp} is[34]

$$a_{pp} = -7.719 \pm .008 \text{ F.}$$

Since the deviations from the accepted p-p scattering length are within the experimental errors, one may conclude that, barring chance compensation of errors in the p-p case, there seems to be no systematic error in the enhancement factors within our experimental accuracy over the energy range used in the determination of the n-n scattering length.

D. Determination of the n-n Scattering Length from the Reaction $\pi^- + D \rightarrow n + n + \gamma$

The outstanding advantage of this reaction in determining the neutron-neutron scattering length is that there is only one final state strong interaction possible. For this reason primarily, this reaction has been studied extensively both theoretically[2-4] and experimentally[5-7] over the years. The most recent work is that of Haddock et al.[7] who used the treatment of Bander[4] to fit their spectra. The enhancement factor obtained by Bander is identical to the Jost function enhancement of (19). Approximately 2000 neutron-neutron coincidences at four opening angles were used to obtain the value of the scattering length

$$|a_{nn}| = 16.4 \pm 1.9 \text{ F}.$$

The value which we have obtained, - 16. 1 ± 1.0 F agrees quite well.

One serious difficulty in the use of this reaction should be pointed out.[36] The primary interaction is the π^- photoproduction from the protons at threshold, about which nothing is known experimentally. If it depended strongly on the n-γ relative momentum, the energy dependence of the n-n final state interaction could be considerably distorted. Unfortunately, empirical evidence against such a possibility, namely the measurement of the p-p scattering length using the mirror reaction, is not readily obtained for this type of experiment.

ACKNOWLEDGMENTS

The author wishes to thank Dr. H. E. Conzett and Dr. R. J. Slobodrian for their generous assistance throughout his experimental work; Professor A. C. Helmholz for his guidance, and Miss Miriam Machlis for her deciphering of my handwriting and typing this manuscript.

APPENDICES

A. Phase Space Energy Dependence

$$\Phi_3 = \frac{1}{h^9}\int d^3p_1 \quad d^3p_2 d^3p_3 \qquad \delta\left(\Sigma p_i\right)\delta\left(\Sigma p_i^{\,2}/2m_i - E_0\right)$$

$$= \frac{1}{h^6}\int d^3p_1 d^3p_2 \; \delta\left(\Sigma p_i^{\,2}/2m_i - E_o\right)$$

$$= \frac{1}{h^6}\int p_1^{\,2} dp_1 d\Omega_1 p_2^{\,2} dp_2 d\Omega_2 \delta\left(\Sigma p_i^{\,2}/2m_i - E_o\right)$$

$$p_1 = p_1(\theta_1, \phi_1)$$

$$d\Omega_2 = p_2^{\,2} \sin\theta_2 d\theta_2 d\phi_2 \; .$$

Integrate over the azimuth $\vec{p}_2$ and the direction of p_1

$$= \frac{8\pi^2}{h^6}\int p_1^{\,2} dp_1 p_2^{\,2} dp_2 d\left(\cos\theta_1\right)_2 \delta\left(\Sigma_i E_i - E_0\right)$$

$$= \frac{8\pi^2}{h^6}\int p_1 p_2 p_3 dp_1 dp_2 dp_3 \; \delta\left(\Sigma_i E_i - E_0\right) ,$$

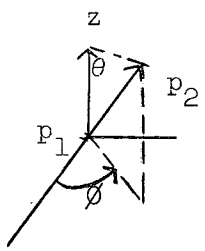

since

$$p_1 p_2 d\left(\cos\theta_{12}\right) = p_3 dp_3$$

$$dE_3 = \frac{p_3 dp_3}{m_3} \qquad dE_2 = \frac{p_2 dp_2}{m_2} \qquad dE_1 = \frac{p_1 dp_1}{m_1}$$

$$\Phi_3 = \left(m_1 m_2 m_3\right) \frac{8\pi^2}{h^6} \int dE_1 dE_2 \quad \text{where} \quad \int dE_3 \delta\left(E_1 + E_2 + E_3 - E_0\right) = 1.$$

$\therefore$ Phase space available to the reaction products is proportional to the area in $E_1 - E_2$ space.

B. Calculation of Jacobian Transformation

It suffices for our purposes to calculate the non-relativistic Jacobian. The transformation follows naturally from the equality

$$\frac{d^2\sigma}{dEd\Omega}\, dEd(\cos\theta) = \frac{d^2\sigma_o}{dE_o d\Omega_o}\, dE_o \left(d\cos\theta_o\right) \tag{B-1}$$

where the sub-index o indicates c.m. variables. Thus, in a more compact form

$$\frac{d^2\sigma}{dEd\Omega} = J\,\frac{d^2\sigma_o}{dE_o d\Omega_o} \tag{B-2}$$

where J is the Jacobian transformation

$$J = \frac{\partial\left(E_o,\ \cos\theta_o\right)}{\partial(E,\ \cos\theta)} \quad . \tag{B-3}$$

The following relations hold between velocities in both coordinate systems

$$v\cos\theta - v_G = v_o\cos\theta_o$$

$$v_o^{\,2} = v_G^{\,2} - 2v_G\, v\cos\theta + v^2$$

where v_G is the laboratory velocity of the c.m.; from these relations we can derive the functional dependence of E_o, $\cos\theta_o$ on E and $\cos\theta$

$$E_o = \frac{1}{2}\, mv_G^{\,2} - 2v_G\cos\theta\sqrt{\frac{2}{m}}\; E^{1/2} + E$$

$$\cos\theta_o = \frac{\left(\frac{2E}{m}\right)^{1/2}\cos\theta - v_G}{\left(\frac{2E_o}{m}\right)^{1/2}}$$

$$J = \begin{vmatrix} 1 - v_G \cos\theta \sqrt{\frac{2}{m}}\, E^{-1/2} & -2v_G \sqrt{\frac{2}{m}}\, E^{1/2} \\ \dfrac{\frac{1}{2}\sqrt{\frac{2}{m}} \cos\theta\, E^{-1/2}}{\left(\frac{2E_o}{m}\right)^{1/2}} + \dfrac{\partial \cos\theta_o}{\partial E_o} \dfrac{\partial E_o}{\partial E} & \left(\dfrac{E}{E_o}\right)^{1/2} + \dfrac{\partial \cos\theta_o}{\partial E_o} \dfrac{\partial E_o}{\partial \cos\theta} \end{vmatrix}$$

The first row of J is precisely $\left(\frac{\partial E_o}{\partial E} \quad \frac{\partial E_o}{\partial \cos\theta}\right)$ and thus the additive terms of the second row are proportional to the terms of the first row, hence can be omitted. The result is simply

$$J = \left(\frac{E}{E_o}\right)^{1/2} \tag{B-4}$$

FOOTNOTES AND REFERENCES

* This work was done under the auspices of the U. S. Atomic Energy Commission.

1. K. Watson, Phys. Rev. 88, 1163 (1952).
2. K. M. Watson and R. M. Stuart, Phys. Rev. 82, 738 (1951).
3. K. W. McVoy, Phys. Rev. 121, 1401 (1961).
4. M.Bander, Phys. Rev. 134, B1052 (1964).
5. R. Phillips and K. Crowe, Phys. Rev. 96, 484 (1954).
6. J. W. Ryan, Phys. Rev. Letters 12, 564 (1964).
7. R. P. Haddock, R. M. Salter, Jr., M. Zeller, J. B. Czirr and D. R. Nygren, Phys. Rev. Letters 14, 318 (1965).
8. E. Baumgartner, H. E. Conzett, E. Shield and R. J. Slobodrian, Phys. Rev. Letters 16, 105 (1966).
9. A. Abashian, N. Booth and K. Crowe, Phys. Rev. Letters 5, 258 (1960).
10. E. Lomon, S. Morris, E. J. Irwin, Jr., and T. Twong, Ann. Phys. 13, 359 (1961).
11. T. Hamada and I. D. Johnston, Nuc. Phys. 34, 382 (1962).
12. D. Y. Wong and H. P. Noyes, Phys. Rev. 126, 1866 (1962); H. P. Noyes, Nucl. Phys. 74, 508 (1965).
13. E. M. Henley and L. K. Morrison, Phys. Rev. 141, 1489 (1966).
14. M. P. Nakada, J. D. Anderson, C. C. Gardner, J. McClure and C. Wong, Phys. Rev. 110, 594 (1958).
15. M. L. Goldberger and K. M. Watson, Collision Theory (John Wiley and Sons, Inc. New York, 1964).
16. John Gillespie, Final-State Interactions (Holden-Day, Inc., San Francisco, 1964) p. 96.

17. C. Williamson and J. P. Boujot, Tables of Range and Rate of Energy Loss of Charged Particles of Energy 0.5 to 150 MeV, Commissariat a L'Energie Atomique Report No. 2189, France (1962).

18. Fred Goulding, Semi-Conductor Detectors for Nuclear Spectrometry, Lawrence Radiation Laboratory Report UCRL-16231, July 30, 1965 (unpublished).

19. F. S. Goulding, D. A. Landis, J. Cerny and R. H. Pehl, Nucl. Instr. and Meth. 31, 1 (1964).

20. T. Lauritsen, F. Ajzenberg-Selove, Energy Levels of Light Nuclei, Nuclear Data Sheets (National Academy of Science, Washington, D. C. 1962).

21. Arthur Springer, Scattering of 50.9 MeV Alpha Particles from Ne^{20} and Ca^{40}, (Ph. D. Thesis) Lawrence Radiation Laboratory Report UCRL-11681, May 6, 1965 (unpublished).

22. O. M. Bilaniuk and R. J. Slobodrian, Physics Letters 7, 77 (1963).

23. E. M. Henley, F. C. Richards, and D. U. L. Yu, Physics Letters 15, 331 (1965).

24. S. T. Butler, Proc. Roy. Soc. (London) A208, 559 (1951).

25. M. Cerineo, K. Ilakovac, I. Slaus, P. Tomas and V. Valkovic, Phys. Rev. 133, B948 (1964).

26. V. K. Voitovetskii, I. L. Konsunskii and Y. F. Pazhin, Physics Letters 10, 109 (1964).

27. R. L. Gluckstern and H. A. Bethe, Phys. Rev. 81, 761 (1950).

28. R. J. N. Phillips, Nuc. Phys. 53, 650 (1964).

29. E. M. Henley and D. U. L. Yu, Phys. Rev. 133, B1445 (1964).

30. V. Ajdacic, M. Cerineo, B. Lalovic, G. Paic, I. Slaus and P. Tomas, Phys. Rev. Letters 14, 442 (1965).

31. T. A. Tombrello and A. D. Bacher, Physics Letters 17, 37 (1965).

32. Paul F. Donovan, Experimental Investigations of Several Few Nucleon Systems, Gatlinburg Conference, Brookhaven National Laboratory Report BNL-8509 (Oct. 1965).

33. R. W. Zurmuhle, Nuc. Phys. 72, 225 (1965).

34. R. J. Slobodrian, Nuovo Cimento 40, 443 (1965).

35. H. E. Conzett, E. Shield, R. J. Slobodrian and S. Yamabe, Phys. Rev. Letters 13, 625 (1964).

36. M. J. Moravcsik, Phys. Rev. 136, B624 (1964).

This report was prepared as an account of Government sponsored work. Neither the United States, nor the Commission, nor any person acting on behalf of the Commission:

A. Makes any warranty or representation, expressed or implied, with respect to the accuracy, completeness, or usefulness of the information contained in this report, or that the use of any information, apparatus, method, or process disclosed in this report may not infringe privately owned rights; or

B. Assumes any liabilities with respect to the use of, or for damages resulting from the use of any information, apparatus, method, or process disclosed in this report.

As used in the above, "person acting on behalf of the Commission" includes any employee or contractor of the Commission, or employee of such contractor, to the extent that such employee or contractor of the Commission, or employee of such contractor prepares, disseminates, or provides access to, any information pursuant to his employment or contract with the Commission, or his employment with such contractor.